LAWRENCE
LIVERMORE
NATIONAL
LABORATORY

LLNL-JRNL-827873

Controls on Plutonium and Americium Release in Subsurface Environments Exposed to Acidic Processing Wastes

H. P. Emerson, S. I. Sinkov, C. I. Pearce, K. J. Kantrell, C. H. Delegard, M. M. V. Synder, M. Thomas, D. D. Reilly, E. C. Buck, L. Sweet, A. J. Casella, J. C. Carter, J. F. Corbey, I. G. Schwerdt, R. Clark, F. D. Heller, D. Beier, M. Zavarin, A. B. Kersting, V. L. Freedman

October 13, 2021

Applied Geochemistry

Disclaimer

Solubility Controls on Plutonium and Americium Release in Subsurface Environments Exposed to Acidic Processing Wastes

Hilary P. Emerson[a], Sergey I. Sinkov[a], Carolyn I. Pearce[a]*, Kirk J. Cantrell[a], Calvin H. Delegard[b], Michelle M.V. Snyder[a]; May-Lin Thomas[a], Dallas D. Reilly[a], Edgar C. Buck[a], Lucas Sweet[a], Amanda J. Casella[a], Jennifer C. Carter[a], Jordan F. Corbey[a], Ian J. Schwerdt[a], Richard Clark[a], Forrest D. Heller[a], David Meier[a], Mavrik Zavarin[c], Annie B. Kersting[c], Vicky L. Freedman[a]

*Corresponding Author

E-mail: carolyn.pearce@pnnl.gov

Pacific Northwest National Laboratory, 902 Battelle Boulevard, P.O. Box 999, Richland, WA 99352

[a]Pacific Northwest National Laboratory, Richland, WA 99352

[b]TradeWind Services, LLC, Richland, WA 99352

[c]Lawrence Livermore National Laboratory, Livermoore, CA 94550

For submission to: Applied Geochemistry

Keywords: Plutonium oxide solubility, Plutonium and americum phosphate, Pu(IV) colloids, pseudocolloids, geochemical modeling

ABSTRACT

To identify the role of waste composition and sediment interactions in controlling Pu and Am mobility in contaminated sediments at Hanford, a legacy nuclear site, Pu and Am concentrations in solutions equilibrated with contaminated sediments from beneath the 216-Z-9 (Z-9) Trench were compared to the solubilities of PuO_2 materials, representative of the disposed wastes, in the absence of sediments. ~~This work shows that the solubilities of PuO_2 materials synthesized by different methods, and with varying particle sizes, agree with PuO_2(am,hyd) present as a coating on PuO_2(cr).~~ According to saturation index (SI) calculations, PuO_2(am,hyd) is likely controlling Pu release under conditions where phosphate concentrations are low. However, both Pu-phosphate and Am-phosphate phases, identified in SI calculations and by high resolution transmission electron microscopy, play roles in controlling release in low pH, high phosphate shallow sediments at the top of the Z-9 Trench. The elevated phosphate is likely due to decomposition of tributyl phosphate over time. Sediments from deeper in the subsurface beneath the Z-9 Trench are less acidic and contain less phosphate, with Pu solubility likely controlled by PuO_2(am,hyd) that precipitated following neutralization of the acidic waste stream. Controls on Am concentration in deeper sediments are more complex and potentially involve sediment adsorption and/or release from $Pu_{(1-x)}Am_xO_2$ following Am in-growth. The concentrations of both Pu and Am were elevated in the colloidal fraction associated with shallow sediments, but not in PuO_2 experiments, suggesting the presence of Pu/Am pseudocolloids (e.g., Pu/Am associated with mineral colloids). However, Pu and Am association with the colloidal size fraction was not observed in deeper sediments, suggesting transport of Pu and Am to these depths beneath the Z-9 Trench was not due to colloidal transport.

1. INTRODUCTION

Plutonium (Pu) and americium (Am) are considered highly toxic contaminants that represent a significant long-term public health risk when released into the environment. Release of Pu has occurred at dozens of locations worldwide, with amounts deposited to the subsurface at individual sites ranging from a few milligrams to hundreds of kilograms (Deblonde et al., 2020). Releases have occurred worldwide from Pu production, processing, and waste disposal at sites including the Savannah River Site in South Carolina, USA; the Mayak Production Association in Russia; and the Hanford Site in southeastern Washington State, USA (Carlton et al. 1992; Corbin et al. 2005; Skipperud et al. 2005; Cantrell and Felmy 2012; Gephart 2010; Delegard et al. 2019). Pu was also released during nuclear weapons testing at the Nevada National Security Site, NV, USA and other weapons testing sites worldwide (Finnegan et al. 2016).

These releases have occurred in hydrogeologic regimes spanning from arid, high deserts to oceanic environments. The source terms also vary from acidic to alkaline pH with significantly different chemical inventories. Thus, the mobility of Pu and Am in these systems is subject to a wide variety of hydrological and geochemical processes. Mechanisms responsible for Pu and Am migration in the subsurface may differ due to variability in pH, Eh, co-disposed and natural metal ions, complexing agents, and their combined effects on oxidation state and speciation. Under environmental conditions, Am is predominantly trivalent, whereas Pu can occur in multiple oxidation states from (III) to (VI) (e.g., Silva and Nitsche, 1995). Pu(V) is primarily present in the aqueous phase, due to its relatively high solubility and low adsorption but is often reduced to Pu(IV/III) upon interaction with sediments (Kaplan et al. 2006). Pu(IV) is the dominant oxidation state in the solid phase due to adsorption and precipitation processes, with low concentrations present in solutions in the absence of complexants ($< 10^{-14}$ M at pH 7 in 1

mM NaCl) due to hydrolysis (Guillaumont et al. 2003). Pu(IV) can also be transported in aqueous or organic phases as: (i) intrinsic colloids generated by Pu(IV) hydrolysis through oxo and/or hydroxyl bridge formation; or (ii) pseudocolloids formed by sorption of Pu(IV) onto colloids composed of other constituents. When $Pu(IV)O_2$ is present, dissolved oxygen may also lead to dissolution and subsequent oxidation to $Pu(V)O_2^+$ or $Pu(VI)O_2^{2+}$ and radiolysis can enhance this oxidation (e.g. Rai et al. 1981; Neck et al. 2007). Pu disposed to the subsurface may also interact with waste co-contaminants and sediments in unique ways to form previously unidentified compounds like Pu-Bi composites (Emerson et al. 2021), Fe-Pu-phosphate minerals (Buck et al. 2014), and Pu incorporated into silica gels (Ames, 1974).

In Pu-bearing waste streams, the concentration of ^{241}Am may increase over time by beta decay of the short-lived ^{241}Pu (half-life of 14.4 years). Am(III) species are generally soluble over a wide range of pH values, depending on available complexants. At acidic waste disposal sites, and in the presence of phosphate, Am can precipitate as relatively insoluble $AmPO_4$(am,hyd) or substitute into other phosphate compounds (Rai et al. 1992). Indeed, a highly insoluble, amorphous precipitate can form by direct mixing of PO_4^{3-} in a dilute, weakly acidic Am^{3+} solution (Rai et al. 1992), although this mechanism has not been directly observed in natural sediments. Additionally, Am may be present as Am(IV) within the $Pu_{(1-x)}Am_xO_2$ structure, or as mixed Am(IV)/(III) in $Pu_{1-y}Am_yO_{2\pm x}$, due to the decay of ^{241}Pu to ^{241}Am in PuO_2 (Vauchy et al. 2017; Emerson et al. 2021; Neilson et al. 2021).

The objective of this research is to determine the solubility-controlling phases for both Pu and Am in contaminated sediments from the Z-9 Trench at the Hanford Site so that their future remobilization potential and risk to groundwater can be predicted (Cantrell and Felmy, 2012; Delegard et al. 2019). Knowledge of Pu and Am migration behavior beneath the Z-9 Trench can

inform the potential for mobilization in other areas of the Hanford Site, including the 216-Z-1A tile field and 216-Z-18 crib that received similar Pu- and Am-laden acidic and high-salt waste (Delegard et al. 2019; Gerber 1997). Mechanisms that control Pu and Am migration following acidic and organic waste releases are relevant to other sites with similar Pu contamination (e.g., Los Alamos, NM and Savannah River Site, SC) (Batuk et al. 2015; Carlton et al. 1992).

The solubilities of different PuO_2 materials, in the absence of sediments under the solution conditions expected in the contaminated sediments, were measured to determine if synthesis method or particle size affected Pu and Am concentrations in solution. Pu and Am solubilities in the absence of sediment were compared with solution phase Pu and Am concentrations measured following equilibration with Z-9 Trench sediments from the Hanford Site to determine the influence of sediments on Pu and Am solubility. Speciation modeling was employed to consider the impact of complexants (e.g., phosphate, carbonate) measured in the aqueous phase following reaction with contaminated sediments. Data for Am and Pu were used to infer their solubility-controlling phases in conjunction with equilibrium solubility calculations.

2. BACKGROUND

2.1 The Hanford Site as a case study for plutonium release and migration

The Hanford Site was established in 1943 in the arid desert of southeastern Washington State to produce Pu for nuclear weapons. Pu was finished by conversion to metal and manufactured into metallic shapes for nuclear weapons at the Plutonium Finishing Plant (PFP) (Gerber 1997). Near-surface disposal of liquid wastes contained an estimated 11,800 Ci (189 kg) of ^{239}Pu; 2,900 Ci (12.6 kg) of ^{240}Pu; 37,500 Ci (0.34 kg) of ^{241}Pu, 28,700 Ci (9.0 kg) of ^{241}Am; and 55 Ci (78 kg) of ^{237}Np with 21 waste sites receiving 97% of the Pu (Cantrell and Felmy 2012). These wastes

were discharged into waste disposal facilities such as trenches, cribs, and anthropogenic ponds (see recent review by Delegard et al. 2019). This includes 5×10^4 Ci or 200 kg of Pu, primarily released from the PFP, with over half of that discharged into the unlined Z-9 Trench.

Sites for waste disposal from Pu processing and finishing at the PFP can be classified into two major categories (Cantrell et al. 2003; Cantrell and Riley 2008; Delegard et al. 2019): (i) low-salt, near-neutral wastes (e.g., off-gas scrubber solutions) and (ii) acidic, high-salt waste that was co-disposed with spent organic solvent extraction solutions. With both waste types, measurable concentrations of Pu and Am reached depths greater than 40 m below ground surface (bgs) in the unsaturated (vadose) zone (Cantrell and Felmy 2012; Delegard et al. 2019). However, Pu and Am concentrations in the deep vadose zone were much higher at sites that received acidic, high-salt waste co-disposed with organic solvents such as at the Z-9 Trench and the Z-1A tile field.

The Z-9 Trench was used from 1955 to 1962 for disposal of over 4 million liters of aqueous and organic liquid waste from the PFP (DOE/RL 2007, Corbin et al. 2005). The estimated inventories of $^{239/240}$Pu, ^{241}Pu, and ^{241}Am are 2,180 Ci (31.6 kg), 1060 Ci (0.01 kg) and 565 Ci (0.18 kg), respectively (decay corrected to 1/2021; Cantrell and Felmy 2012). The wastes disposed to the Z-9 Trench were solely from the RECUPLEX Process, which operated at Hanford's PFP from 1955 until 1962 (Judson 1958; Gerber 1997). The Pu-bearing scrap processed by RECUPLEX included Pu(IV) oxalate filtrates, off-specification PuO_2, PuF_4 from failed reductions, off-specification metal, and metal machining swarf and cutting fluids. The raffinates from RECUPLEX were further treated by a second (DBBP) solvent extraction process. The resultant aqueous wastes were partially neutralized to pH ~2.5 and discharged with TBP solvent wash breakdown product wastes, coincident solvent losses, and Pu metal machining fluids to the enclosed Z-9 Trench (Judson et al. 1956). Large (> 1 μm), dense particles of PuO_2

from burnt Pu metal with other undissolved PuO_2 in the RECUPLEX wastes were likely transported by interfacial "cruds" formed from TBP breakdown products.

Concern over the potential for accumulation of a critical mass of Pu on the floor of the trench prompted additional sampling and excavation from 1976-1978 (Smith 1973; Delegard et al. 2019). Sediment samples from a 3-m depth profile of the Z-9 Trench collected prior to excavation contained relatively high Pu and Am concentrations with up to 1×10^{12} pCi/L-sediment (19 g/L-sediment) and 1×10^{11} pCi/L-sediment (41 mg/L-sediment), respectively (Price and Ames 1975). The sediment pH was 4.1 at a depth of 2.4 m (8 ft) and generally acidic through the entire 3 m (9 ft) sediment profile (Smith 1973). After identification of a dense nonaqueous phase liquid at the northeast corner of the Z-9 Trench in the 1990s, additional boreholes were drilled near and under the Z-9 Trench from 2004 to 2006 to define the subsurface contamination (DOE/RL, 2007; BHI, 1995). Analysis indicated that Pu and Am migrated deep (> 40 m bgs) into the subsurface below the trench, likely facilitated by the low initial pH of the disposed waste, with some accumulation in or above silt and clay layers (Cantrell and Felmy 2012; Cantrell et al. 2008).

Rai et al. (1980) analyzed the Z-9 sediment samples (4-11A and 4-5A) collected from the bottom of the trench and suggested that some Pu was present as PuO_2. X-ray diffraction (XRD) and electron microprobe analyses showed that Pu was discharged as both particulate PuO_2 (up to 84 wt.% Pu in individual particles) and dissolved phases with bulk sediment (Ames 1974, Rai et al. 1980; Corbey et al. 2019). The particulate PuO_2 was mostly filtered out within the first meter of the trench sediment, thus accounting for the high concentrations of Pu observed in the upper sediment profile. Near-surface minerals also underwent silicate hydrolysis from interaction with the acidic, high ionic strength wastes and may have sequestered additional Pu and Am (Ames

1974). Pu disposed originally as dissolved Pu(IV) (< 0.5 wt. % PuO_2) penetrated deeper beneath the trench and interacted with sediment. Pu concentrations also correlated with high organic carbon and phosphorus content, presumably from carbon tetrachloride, metal machining fluids, TBP, and DBBP in the waste. Localized peak concentrations of $^{239/240}Pu$ (115 nCi/g) and ^{241}Am (324 nCi/g) were measured previously at 19.4 and 14.5 m bgs, respectively (Cantrell and Felmy, 2012).

2.2 Solubility-controlling Pu and Am phases

PuO_2 has been identified as the major form of Pu within sediments collected from just below the bottom of the Z-9 Trench (Swanson 1973; Ames 1974; Price and Ames 1975; Rai et al. 1980; Buck et al. 2014; Corbey et al. 2019; Emerson et al. 2021). The recommended solubility constant for aged amorphous oxide and hydroxide PuO_2(am, hyd) at zero ionic strength is (Lemire et al. 2001; Guillaumont et al. 2003):

$$PuO_{2(am,hyd)} + 2H_2O = Pu^{4+} + 4OH^- \quad \log K^o_{s,0}\ (298.15\ K) = -58.33 \pm 0.52 \quad (1)$$

Over time, PuO_2(am,hyd) never completely crystallizes under aqueous, low temperature conditions, likely due to radiolysis counteracting Ostwald ripening (Rai and Ryan 1982).

Previous work has suggested that the chemical history, physical form, and other fundamental properties of PuO_2 can influence Pu dissolution and re-precipitation processes. Zhao et al. (2020) showed that PuO_2 formed under acidic conditions was more ordered, more stable and less likely to dissolve than PuO_2 formed under alkaline conditions, even though both had similar particle sizes. Rai et al. (1980) showed that $Pu(OH)_4$, prepared by rapid precipitated from Pu(IV) nitrate solution with sodium hydroxide, maintained a higher Pu concentration in solution at environmental pH than PuO_2 microspheres (~150 μm diameter and ~100 nm crystallite size), prepared by sol-gel techniques and calcined to 1150 °C (Lloyd and Haire 1968), but that a linear

relationship existed between pH and total Pu concentration in solution in equilibrium with the different Pu compounds (Rai et al. 1980). Kanellakopulos et al. (1983) studied the behavior of PuO_2(cr) with varying crystallite sizes, prepared by firing Pu(IV) oxalate at different temperatures, and showed that there was an inverse correlation between the solubility of PuO_2(cr) in nitric acid and the average size of the particles. This previous work suggests crystallinity and particle size can affect PuO_2 solubility, but there has not been a systematic study of PuO_2 solubility, as a function of particle size and synthesis method, under the solution conditions expected in contaminated sediments. As ^{241}Pu decays to ^{241}Am with the PuO_2 structure to form $Pu_{(1-x)}Am_xO_2$, Am release from these particles may also be dictated by surface area and particle size.

Pu solubility is controlled by PuO_2 near the surface of the Z-9 Trench (Rai et al. 1980), but solubility controls may change with depth and time as complexants become available (e.g., degradation of TBP to phosphate) and solid phases react with high ionic strength, acidic waste solutions (e.g., formation of silica gel from acid attack of minerals). Other potential Pu solubility-controlling phases, such as Fe-Pu-phosphate, have been identified in shallow sediments (Buck et al. 2014; Corbey et al. 2019; Emerson et al. 2021), but the amount of Pu present in the deeper sediments is too small for solid phase identification.

To deconvolute solubility controls based on the PuO_2 characteristics (e.g., crystallinity and surface area) and on reactions with the sediments (e.g., secondary mineral transformations) and waste components, the solubility of PuO_2 prepared by methods similar to historical Hanford operations [calcining Pu(III) oxalate to 650 °C and oxidizing Pu metal to ≥ 450 °C] was compared to Pu solubilized from contaminated Hanford Site sediments. As the solubility-controlling Pu and Am phases could not be identified in deeper subsurface sediments, batch

experiments were conducted to generate supernatant for ultra-trace solution phase analysis to infer the Am and Pu solubility controlling phases from equilibrium solubility calculations.

3. MATERIALS AND METHODS

Batch experiments were conducted to determine the solubility controlling phases for Pu and Am. Sediments contain both small, disordered PuO_2 particles, and more crystalline, micron sized PuO_2 particles, indicative of unique synthesis history of Pu particulate material (Corbey et al. 2019; Emerson et al. 2021). The solubilities of PuO_2 particles with different sizes and synthesized by different methods (described in Section 3.2) were determined in the absence of sediments, then compared with Pu solubility in sediments under similar pH and background electrolyte conditions. For Pu analysis, supernatant solutions were allowed to settle overnight, acidified, then filtered to remove any remaining particulates. A subset of supernatant solutions was allowed to settle overnight, then filtered prior to acidification, and the Pu concentrations were compared with those in the solutions acidified pre-filtration to estimate the amount of Pu and Am associated with colloidal particles. Solutions were analyzed for total Pu and Pu(V) concentrations by solvent extraction (Supplemental Materials, SM, Section 1.2.5). Separations were conducted for ultra-trace isotopic analysis for $^{238/239/240/241/242}$Pu and ^{241}Am. In addition, supernatants were analyzed for major anion, cation, and metal concentrations. Results were compared via calculation of saturation indices (SIs) with Geochemist's Workbench® (GWB) as described in Section 3.6.

3.1 Hanford Site Sediments

Table 1 lists the sediment samples used in this study along with relevant depth and sample identification designations. The Z9-4-11A and Z9-4-5A samples were collected by Atlantic

Richfield Hanford Company from below the trench in 1973 (10.2 cm diameter by 14.2 cm long core segments, 60 cm total core length), prior to excavation of the top 0.3 meters of contaminated sediments in 1976-1978 (Swanson 1973; Ames 1974). The 'A' signifies that this sediment was from the top 15 cm of the core. These sediments were homogenized, sieved to remove particles greater than 2 mm, air-dried, and stored at room temperature. Sample Z9 4-11A contains some fraction of an overlying sludge that collected near the trench bottom during waste disposal, consisting of silica and aluminum and with an approximate water content of 35% by weight upon coring (Swanson 1973; Smith 1973; Delegard et al. 2019). The average Pu and Am mass concentrations in Z9-4-11A and Z9-4-5A are shown in Table 1. The B1HK samples were collected in 2006 from slant borehole well 299-W15-48 (C3427) drilled at an angle of 32° from vertical to a depth of 44.3 meters (Cantrell et al. 2008). The B1HK samples were passed through a 53-µm sieve prior to storage at room temperature.

Table 1: Pu-contaminated Z-9 sediment samples used for batch experiments.

Sample ID	Depth Downhole	Depth (meters)	Pu (µg/g)[3]	^{241}Am (µg/g)[4]	Description of Sample
Z9-4-5A	-	0 – 0.15 bbt[1]	851	3.5	Z-9 sediment from bottom of trench
Z9-4-11A	-	0 – 0.15 bbt	1610	6.7	Z-9 sediment from bottom of trench
B1HK27	67 – 69	17.3 – 17.8 bgs[2]	NR[5]	NR[5]	Z-9 slant borehole sediment
B1HK42	118.5 - 120.5	30.6 – 31.2 bgs	NR[5]	NR[5]	Z-9 slant borehole sediment

[1]below bottom of trench [2]below ground surface [3](Swanson 1973) [4](Rai et al. 1981) [5]NR = not reported

3.2 PuO_2 Synthesis and Characterization

To simulate the PuO_2 disposed to the Z-9 Trench, PuO_2 was prepared in two ways: (i) calcining Pu(III) oxalate; and (ii) furnace oxidation of Pu metal at 400 °C. PuO_2 particles produced from calcined Pu(III) oxalate, and from calcined Pu(IV) oxalates in historical Hanford production, have the same structure and chemistry, and have similar specific surface area, crystallite size, and particle size, as determined by equivalent circular diameter, Brunauer–Emmett–Teller

specific surface area, XRD, and scanning electron microscopy (SEM) with energy dispersive x-ray spectroscopy (EDS) (see Table 2 and SM Section 1.1 for details). The PuO_2 from burnt metal also representative of that produced by historical methods, within the limitations of lab-scale synthesis (gram-scale in the lab, up to kilogram-scale in the plant).

3.2.1 Precipitation of plutonium (III) oxalate and calcination to PuO_2

The plutonium (III) oxalate was prepared batchwise according to Equation 3 and calcined to produce PuO_2 on a plutonium processing testbed.

$$2\ Pu^{3+} + 3\ H_2C_2O_4 + 10\ H_2O \rightarrow Pu_2(C_2O_4)_3 \cdot 10H_2O_{(solid)} + 6\ H^+ \quad (3)$$

Two batches of PuO_2 were produced via Pu(III) oxalate process. The Pu(IV) nitrate feed for both batches was reduced to Pu(III) using ascorbic acid and stabilized with hydrazinium nitrate. Oxalate precipitation for the two respective batches was carried out by: (i) rapid addition of solid oxalic acid with stirring at 30 °C (labelled 'Ox-A'); and (ii) reverse-strike addition of Pu(III) solution to a vessel containing oxalic acid solution with stirring at 50 °C over a period of 20 minutes (labelled 'Ox-B'). Each oxalate suspension was digested, the precipitates vacuum filtered, washed, and air dried. The dried precipitates were calcined to the oxide in a platinum crucible at 650 °C. Ox-A PuO_2 had a smaller particle size but lower specific surface area, and Ox-B PuO_2 had a larger particle size but higher specific surface area.

3.2.2 Oxidation of Pu metal to PuO_2

A Pu metal slice (~1 g) from a button made from legacy Hanford PuF_4 was pickled in nitric acid to remove the pre-existing oxidized layer, washed with water and ethanol, and air dried before furnace oxidation at ≥ 400 °C. This PuO_2 produced by Pu metal oxidation (labelled 'Mt') is broadly representative of metal self-burning in the plant.

3.3 Batch contact experiments with PuO_2

Batch contact experiments were conducted with Ox-A, Ox-B, and Mt PuO_2 in 0.01 M $NaNO_3$ at three initial pH values (3.0, 4.0, and 5.0), acidified using HNO_3 to maintain ionic strength similar to sediment experiments described in Section 3.4. Experiments were conducted in triplicate in 20 mL glass scintillation vials, with ~0.020 g of PuO_2 and 10.0 mL of solution. All suspensions were exposed to air to represent Hanford Site vadose zone conditions. Additional details of the solubility experiments are provided in Table S2.

Experiments were conducted for 30 days on a benchtop shaker, with PuO_2 Mt samples subjected to a second sequential contact period of 90 days with fresh solution to confirm equilibrium. After this time, the samples were gravity-settled overnight, the pH (Hanna HI4521 meter and Accumet 2248056P electrode) and Eh (Mettler Toledo 5134203, reported in mV with respect to a standard hydrogen electrode, SHE) of each solution were measured, and aliquots were removed for subsequent analyses. For two of the triplicates, solutions were separated using 3,000-Da molecular weight cut-off (MWCO, Vivaspin 20, polyethersulfone, PES) centrifugal filters. After filtration, aliquots were retained for: (i) Pu and Am isotopic analyses ($^{239/240/241}$Pu and ^{241}Am) by inductively coupled plasma mass spectroscopy (ICP-MS) (2.0 mL); (ii) extraction into di-(2-ethylhexyl)phosphoric acid (HDEHP) for Pu(IV/VI) oxidation state analysis (0.8 mL); and (iii) major elements by inductively coupled plasma optical emission spectroscopy (ICP-OES) (2.0 mL). Concentrated HNO_3 (25 μL) was added to aliquots (2.0 mL) for Pu/Am isotope and major elemental analyses.

The third sample (labelled ‘B’) was used to determine the total dissolved and colloidal Pu in the supernatant. An aliquot was removed for anion analysis, then the remaining solution was decanted into a centrifugal filter (Vivaspin 20, 3,000-Da MWCO PES) and concentrated HNO_3

(25 μL) was added and thoroughly mixed *prior* to filtration by centrifugation. After filtration, aliquots were retained for Pu and Am isotopic analysis ($^{239/240/241}$Pu and ^{241}Am), and major elements by ICP-OES.

3.4 Batch contact experiments with Z-9 Trench Sediments

Batch contact experiments were conducted with three sediments taken from the Z-9 Trench: (i) 5A, containing large particles of PuO_2 (Z9-4-5A; about 2.5 meters from the original discharge pipe); and (ii) 11A, containing smaller particles of PuO_2 (Z9-4-11A; about 14 meters from the discharge pipe), and (iii) deeper sediments from below the Z-9 Trench (B1HK-27 and B1HK-42, Table 1). All suspensions were exposed to air to represent Hanford Site vadose zone conditions.

The first set of experiments was conducted with 10 g of the deeper sediments (B1HK27 and B1HK42) or 0.5 g of the shallower sediments (Z9-4-5A and Z9-4-11A) in deionized water (DIW, 20 mL), as shallow sediments contained much higher Pu concentrations. Experiments were conducted in 50-mL centrifuge tubes (polypropylene, Corning) and mixed on a benchtop shaker at 6 rpm for 8 days. The B1HK27 and B1HK42 samples were conducted in triplicate, while the Z9-4-5A and Z9-4-11A samples were conducted in duplicate due to limited sample quantities. No pH adjustments were made to represent equilibration with sediments.

A second set of experiments was conducted in triplicate with the trench bottom sediments (Z9-4-5A and Z9-4-11A) using 0.1 g of sediment and 10 mL of DIW in 20 mL glass liquid scintillation vials. Experiments were conducted under two conditions: (i) pH adjusted to 3.0 to represent initial release conditions; and (ii) no pH adjustment to represent equilibration with sediments. The samples were equilibrated for 30 days or 90 days, then sampled as described in Section 3.3.

After the contact period, the solution vials were centrifuged (10 minutes at 2000 rpm, 268 relative centrifugal force; Allegra X-22, Beckman Coulter) and then the solution pH (Hanna HI4521 meter and Accumet 2248056P electrode) and Eh (Mettler Toledo 5134203) were measured. This centrifuge step removed particles of approximately 450 nm according to Stoke's law. Two aliquots were then collected for alkalinity and anion analysis (as described in SM Sections 1.3.3 and 1.3.4). A third and fourth aliquot was used to determine the presence of any colloidal Pu that remained suspended in the supernatant but did not pass through the 3,000 Da MWCO filter (< 2.5 nm). The third sample was acidified with concentrated HNO_3 and then filtered with a 3,000 Da MWCO centrifugal filter (PES, Vivaspin). The fourth sample was filtered through 3,000-Da MWCO centrifugal filters and then acidified with concentrated HNO_3. Metals were analyzed by ICP-MS and ICP-OES.

3.5 Analytical methods

3.5.1 Isotopic separation and analysis

Measurement of the Pu and Am isotope concentrations required a separation procedure to prevent isobaric interferences (e.g., ^{241}Pu and ^{241}Am). Aqueous supernatants were first screened by ICP-MS using ^{233}U as a pseudo-isotope dilution to estimate levels of matrix elements that may cause interferences, and to determine the appropriate mass loading and analyte concentration. For ^{239}Pu analysis, an aliquot of the sample solution containing <250 pg ^{239}Pu was spiked with 10 pg ^{244}Pu and digested to adjust the sample solution aliquot to a final matrix of 3 M HNO_3. Ascorbic acid and sodium nitrite were added sequentially to fix the oxidation state of Pu to Pu(IV). The digested solution was loaded onto a Teva column (Eichrom®), which was then eluted to remove the matrix elements. Pu was stripped from the column with dilute hydrochloric acid and brought to a final volume of 5 mL with DIW.

^{241}Am analyses were conducted on a separate aliquot of sample solution because (i) the ^{244}Pu tracer contains ^{241}Am and (ii) the disparity between the Pu and Am concentrations required different dilutions. An aliquot of the sample solution containing < 250 pg ^{241}Am was spiked with 25 pg ^{243}Am and digested to adjust the sample solution aliquot to a final matrix of 3 M HNO_3. Ascorbic acid and sodium nitrite were added to fix the oxidation state of Pu to +4. The digest was loaded onto a Teva-UTeva-TRU (Eichrom®) triple column stack and washed to retain some of the interfering elements onto the Teva and UTeva columns and Am onto the TRU column. The TRU column was detached from the column stack and eluted to remove matrix elements. The Am was stripped from the column with dilute hydrochloric acid, which strips the +3 oxidation state of Am but leaves the +4 oxidation state of Pu on the column, and adjusted to a final volume of 5 mL with DIW. Instrument detection limits were 1.6×10^{-6} µg/L for Pu isotopes and 1.0×10^{-6} µg/L for ^{241}Am.

3.5.2 Pu oxidation state separation

Oxidation state analysis of Pu by organic extraction by HDEHP has been described previously (Powell et al. 2004). Briefly, approximately 0.8 mL of sample solution was added to a vial with 0.2 mL of 5.0 M HCl. Then, 0.5 mL of 0.5 M HDEHP dissolved in hexane (and previously equilibrated with 1 M HCl) was added to the plastic vial. The suspension was mixed for three minutes and then separated by centrifugation. The aqueous phase was analyzed for ^{239}Pu as described in Section 3.5.1 without isotopic separations to estimate the total Pu(V) in solution.

3.6 Geochemical modeling

Thermodynamic equilibrium modeling was used to calculate solution speciation and mineral SIs for solid phases potentially in equilibrium with the supernatant compositions. The SI is defined

as log (Q/K_{sp}), where Q is the activity product and K_{sp} is the mineral solubility product at equilibrium at the temperature of interest. In general, minerals with SI values of zero are at equilibrium where more positive values are considered oversaturated and more negative values are considered undersaturated with respect to the pertinent solid phase. Therefore, SI values from 0 to approximately 1 will be considered saturated in modeling outputs. GWB version 10.0 (Bethke and Yeakel 2010) was used for the modeling. Calculations were performed using the thermodynamic database file thermo.com.V8.R6+.dat that is supplied with GWB but augmented with the selected data from the Organization for Economic Co-operation and Development/Nuclear Energy Agency-Thermochemical Database Project (NEA TDB) (Lemire et al. 2001, Guillaumont et al. 2003; Guillaumont et al. 2020).

3.7 Solid Phase Characterization

The Z9-4-11A and Z9-4-5A samples were analyzed by SEM-EDS (SM Section 1.1 for details). In addition, scanning transmission electron microscopy (STEM) analysis was conducted using a JEOL GrandARM 300F Electron Microscope (JEOL Inc., Japan) equipped with dual energy dispersive x-ray spectrometers operated at 300 kV. Samples for STEM were prepared by embedding Pu-containing Z9-Crib particles in Spurr's resin blocks and thin-sectioning with a Leica UltraCut Ultramicrotome. Principal Component Analysis (PCA) of the STEM-EDS elemental mapping data was performed to isolate the Pu-containing regions. PuO_2 materials were characterized by XRD, Brunauer – Emmett – Teller specific surface area, and SEM as described in SM Section 1.1.

4.0 RESULTS AND DISCUSSION

4.1 PuO_2 samples for solubility studies

XRD analysis for the PuO_2 samples (Ox-A and Ox-B, Mt) confirmed that all samples were crystalline PuO_2 (SM Figure S2). The physical characteristics of the samples are provided in Table 2. The crystallite size, determined from the peak integral breadth of the Lorentzian type convolution to the peak shape in the XRD patterns (see SM Section 1.1.2), was similar for all three samples (13-15 nm). However, the aggregate particles sizes, determined by SEM, differed with Pu-Ox-A being the smallest and Mt being significantly larger than both Pu-Ox materials, <10 μm and >100 μm, respectively (Figure 1). Ox-A was light in color and had a smaller aggregate particle size (Table 2 and Figure 1a) but lower specific surface area (10.39 m^2/g). The smaller aggregate particle size and lower surface area suggest that the crystallites are more densely packed in this sample. Ox-B was dark in color with a larger particle size (Table 2 and Figure 1b) but higher surface area (14.08 m^2/g), suggesting a more open structure. Mt exhibits the 'petrified wood' morphology associated with burnt Pu metal (Figure 1c). The Mt sample morphology was variable, including some particles with a more rounded or square shape, although all particles had surface cracks consistent with Figure 1c. Table 2 also includes the physical characteristics of Hanford PuO_2 produced from the decomposition of Pu(IV) oxalate, showing a similar range for the particle diameter, crystallite size, and surface area as the samples Ox-A and Ox-B samples produced from Pu(III) oxalate.

For comparison, SEM analyses of Z9-4-5A and Z9-4-11A sediments are shown in Figure 2. There are different morphologies of discrete PuO_2 aggregates that range in size from sub-micron to over 20 μm in length, with more large particles present in Z9-4-5A, as discussed in Emerson *et al.* (2020). Thus, the Pu aggregate particle size range is similar to that covered by Ox-A, Ox-B, and Mt. The 'petrified wood' morphology (Figure 1c) consistent with the morphology of the PuO_2 from oxidation of Pu metal, is observed in some of the sediments (Figure 2).

Table 2: Physical properties for PuO_2 from Pu oxalate calcination and Pu metal burning

PuO_2 Source	**Calcination Temperature (°C)**	**Equiv. Circular Diameter (μm)**	**Crystallite Size, nm**	**Spec. Surface Area (m^2/g)**	**Uncertainty (m^2/g)**
Ox-A	650	3.1	13	10.39	0.03
Ox-B	650	8.7	13	14.08	0.11
Mt	400	–	15	–	–
Hanford PuO_2 from Pu(IV) Oxalate	400-425	95% <20 μm, 90% <9-12 μm, 50% <5 μm	4.2, 4.2, 15.5, 15.5, 19.7	48.9, 41.2	–
	650	N/A	22	5.9, 12.8	–
Reference	–	A	B	C	–
Burnt metal	>500	Bimodal, maxima at ~30 μm and 600 μm; 50 mass% <500 μm	unknown	unknown	
Reference		D			

A - Greintz and Neal 1978
B - 400-425°C – Moseley and Wing 1965; 650°C – Kanellakopulos *et al.* 1983 (not specific to Hanford processes)
C - Barr *et al.* 1970
D - Haschke 1992
N/A - Data not available

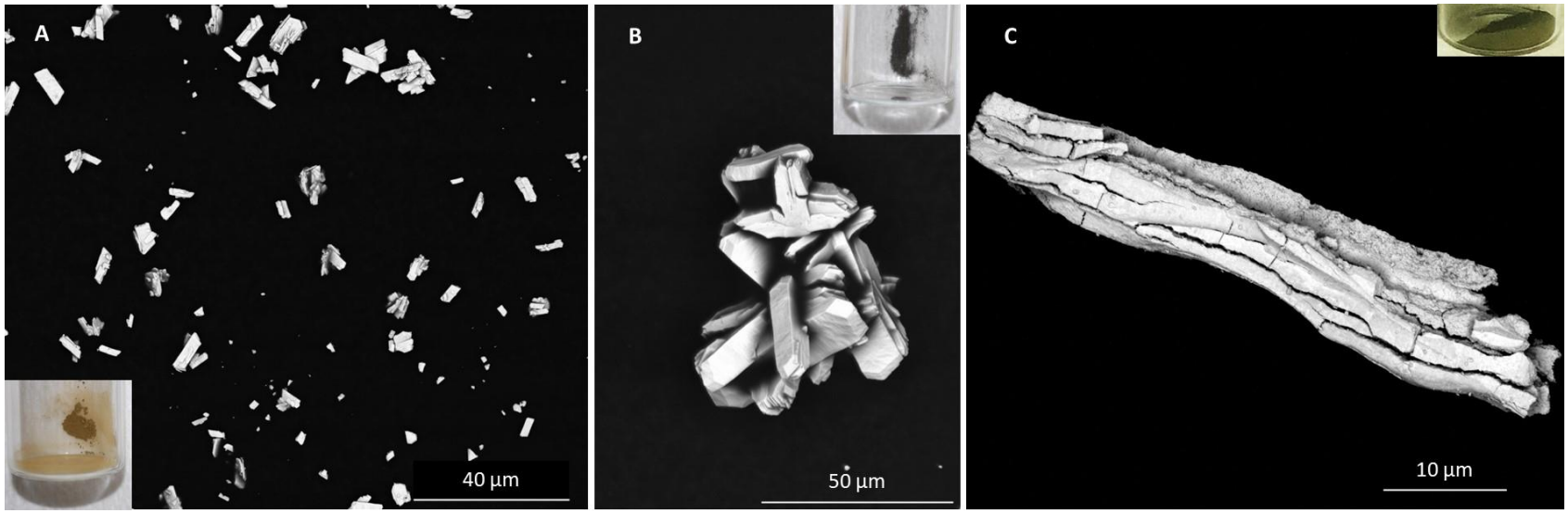

Figure 1: SEM images with inset optical photograph for (A) Ox-A PuO_2 and (B) Ox-B PuO_2 from Pu(III) oxalate calcination, and (C) PuO_2 from oxidation of Pu metal (Mt).

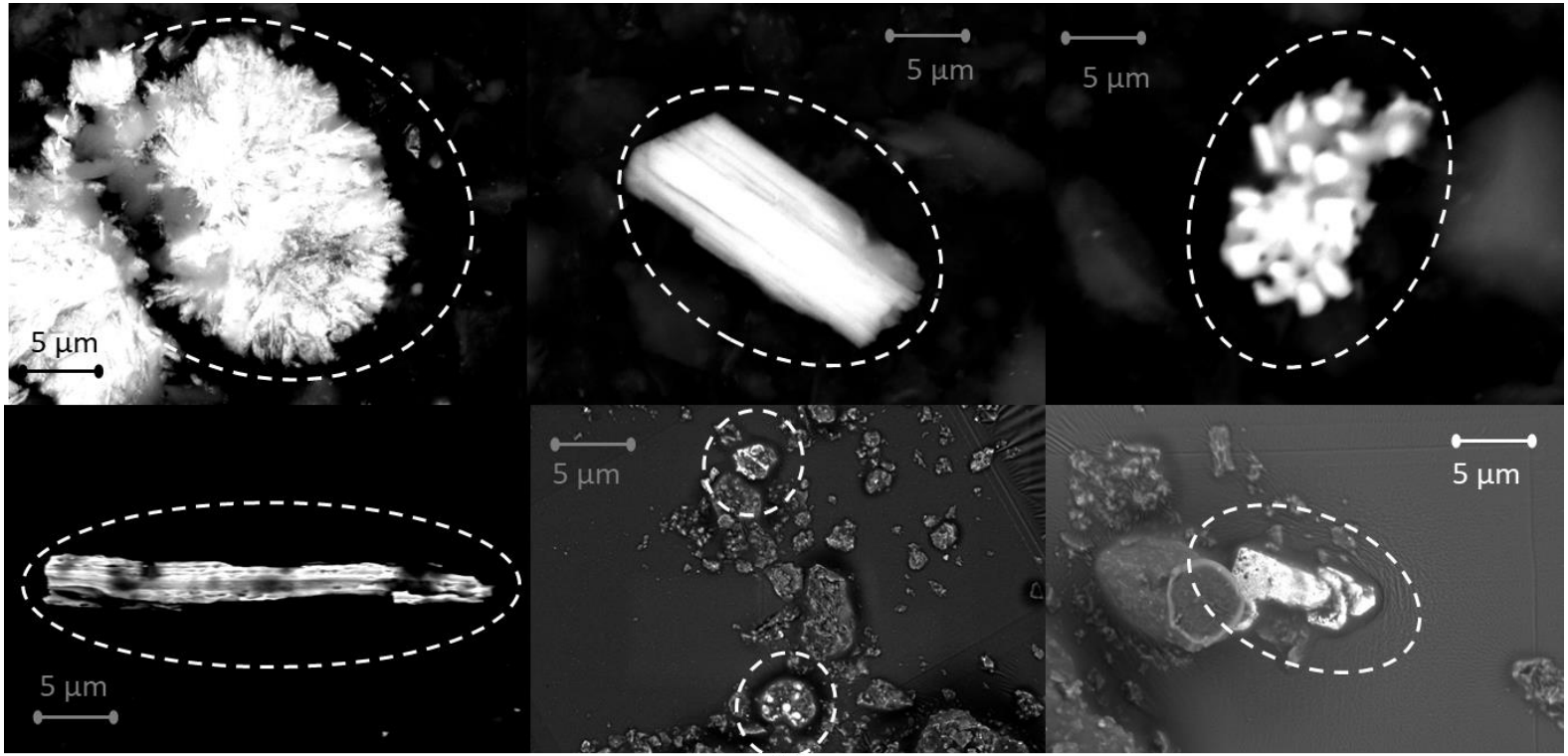

Figure 2: SEM images of Pu in sediments; *top* – Z9-4-5A and *bottom* – Z9-4-11A; dashed, white lines denote particles with high Pu content as observed by EDS (SM Figure S3).

4.2 Solubility of PuO_2

Eh versus pH results from PuO_2 solubility experiments in the absence of sediments fall within the range of PuO_2(am,hyd) based on speciation modeling – *dashed-dot gray line* represents solubility line for PuO_2(am,hyd) under experimental conditions in Figure 3a (SIs shown in SM Tables S9 and S10) and are similar to those found by Rai et al. (1980) in 0.0015 M $CaCl_2$ – *black dashed line* in Figure 3a. The thermodynamic constant for PuO_2(am,hyd) was based on the NEA TDB critical review (Guillaumont et al. 2003; Neck and Kim 2001). In addition, the slope of Eh vs. -Log(Pu) and Eh vs. pH are close to -59 mV (slope of -58 and -48, respectively) which is consistent with a one electron redox process per the Nernst equation, highlighting that Pu(IV) oxidation to Pu(V) is likely occurring during dissolution (SM Figure S8). Aqueous Pu concentrations versus pH for PuO_2 synthesized via oxalate (Ox-A and Ox-B) after the 30-day equilibration period are consistent with Rai *et al.* (1980) (Figures 3a and 4a), even though the crystallite sizes (100 nm versus 15 nm) and aggregate particle sizes (150 μm versus < 10 μm) were substantially different (Table 2).

After the initial 30-day equilibration with PuO_2 synthesized by oxidation of Pu metal (Mt), the pH of solutions initially at 4 and 5 increased to 6.1-7.2 (SM Figure S5). This pH increase is likely a result of neutralization of trace amounts of CaO, present due to the oxidation of trace Ca metal remaining from the calciothermic reduction process. Ca contamination was qualitatively confirmed via SEM-EDS analysis of the Mt solid (SM Figure S3), and quantitative ICP-OES results confirmed that Ca was present in solution (30.1 ± 9.7 mg/L in Mt), however the consumption of H^+ by CaO versus Pu dissolution could not be differentiated. Over the pH range from 3.1 to 7.2, aqueous Pu concentrations for Mt were lower than Ox-A and Ox-B at 30 days (Figure 4a and with Pourbaix diagrams overlaid in SM

Figure S7 and SIs in Table S9 and S10). It is possible that these lower aqueous Pu concentrations are due to the lower surface area of Mt material (Figure 1c) requiring longer equilibration time. Therefore, fresh 0.01 M $NaNO_3$ solutions were added after the initial 30 days, the pH adjusted to 3, 4, and 5, and equilibration was continued to 90 days to confirm that equilibrium was reached. Over the subsequent 90-day interval, the pH did not shift as much for the pH 4 and 5 tests.

The difference in time to reach equilibrium; 30 days for the smaller PuO_2 particles produced by a sol-gel method with calcination (Rai et al., 1980) and by calcination of Pu(III) oxalate, versus 90 days for the larger PuO_2 produced by oxidation of Pu metal (Figure 4a), confirm previous findings that crystallite size and surface area play a role in PuO_2 dissolution rates (Kanellakopulos et al. 1983). However, a significant effect on solubility under acidic conditions has not been identified here. As expected, these results most closely agree with PuO_2(am,hyd) solubility associated with less crystalline (or microcrystalline) coatings on PuO_2 (Rai and Ryan 1982) as shown in Figure 3 and SM Tables S9 and S10.

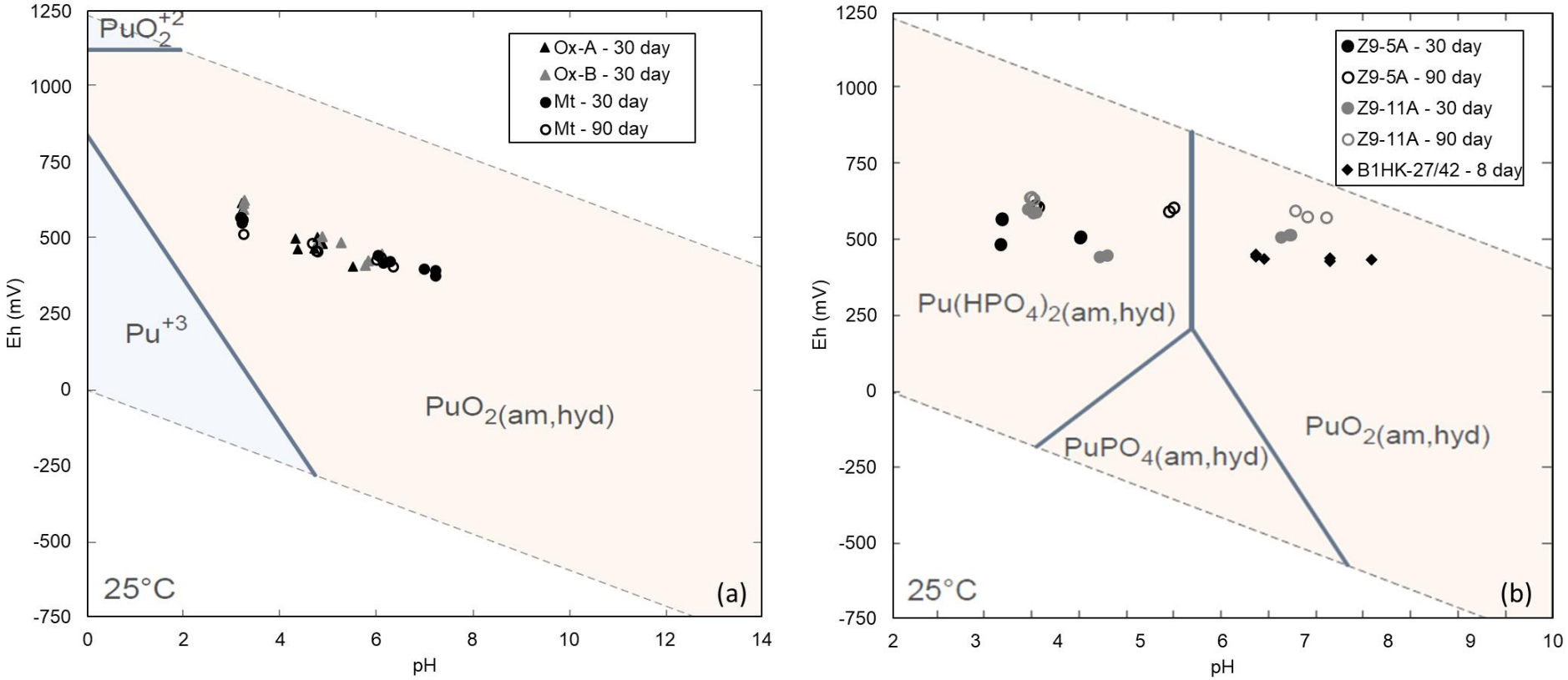

Figure 3: Pu stability field diagram based on analytical characterization of aqueous supernatants from 30-day batch solubility experiments with (a) PuO_2 solubility experiments (Pourbaix diagram based on sample Ox-B-3BF, 6×10^{-6} M Pu in 10 mM $NaNO_3$) and (b) Pu-contaminated sediments from Z-9 Trench (Pourbaix diagram based on sample Z-9-4-11A-6BF, 2.3×10^{-7} M Pu with major components measured in solution) where *blue* regions represent dominant aqueous species and *yellow* regions represent solid phase species as labeled. Note: Major constituents included from a

specific sample from each set, although predicted Pourbaix diagrams were similar for all conditions for PuO_2 and Pu-contaminated sediments, respectively. In addition, carbonate was excluded from this system. In equilibrium with air, carbonate species are not dominant until pH > 10 and, therefore, are not relevant to this study (see SM Figure S7a).

4.3 Pu and Am solubility-controlling phases in contaminated sediments

Sediments from beneath the Z-9 Trench were equilibrated with DIW for 7-, 30-, and 90-days (Figure 4b,c). Similar aqueous Pu and Am concentrations were obtained for equilibration of Z-9 Trench sediments with 0.0015 M $CaCl_2$ solutions, up to 250 days and 707 days respectively (Rai et al. 1980; 1981), therefore, we expect that equilibrium was reached within the 90-day timescale of these experiments. The SIs calculated for potential Pu and Am phases are shown in Tables 3 and 4. Samples that were acidified after filtration (AF) and before filtration (BF) represent Pu associated with dissolved (AF) and combined dissolved and colloidal species (BF). Total Pu, ^{241}Am, and phosphate concentrations are presented along with pH and Eh (Tables 3 and 4). Additional components included in the GWB calculations are in the SM Tables S5-S7 with all SIs shown in SM Tables S8-S10.

The supernatant from the shallow Z9-4-5A and Z9-4-11A samples had higher aqueous Pu, Am, and phosphate concentrations compared to the deeper samples (B1HK-27/42, shown in Figure 4b,c and Tables 3-4 and SM Table S3); and they were more acidic, reflecting the acidic waste in contact with shallow trench sediments. The Z9-4-5A supernatant had lower pH and higher phosphate concentrations than the Z9-4-11A, whereas the Z9-4-11A had higher aqueous Pu and Am concentrations than the Z9-4-5A samples. The pH increased with the second equilibration (90 days) for Z9-4-5A suggesting some loss of acid capacity with the first equilibration step for 30 days (SM Figure S5).

Although solution redox conditions for Z9-4-5A sediments (30 days) were similar to those for PuO_2 solubility experiments in the absence of sediments, redox conditions for Z9-4-5A (90 days), Z9-4-11A, and B1HK sediments became more oxidizing over time (Section 4.2, SM

Figure S4). This indicates that PuO_2, and associated alpha radiolysis, are not be the sole control on redox in these sediments.

4.3.1 Pu solubility-controlling phases in contaminated sediments

Aqueous, dissolved Pu concentrations in Z-9 Trench sediments (4b,c *filled* symbols) are well below the range of PuO_2 solubility in the absence of sediments (Figure 4a). This highlights the influence that sediments and waste components have on Pu solubility as well as the complex sorption processes with sediments. The shallow Z-9 Trench sediments (Figure 4b) contain large, well-ordered, crystalline PuO_2 particles (Z9-4-5A), and smaller, less ordered PuO_2 particles (Z9-4-11A), as shown previously by autoradiography, electron microprobe analysis, SEM and EXAFS (Ames, 1974; Rai et al. 1980; Felmy et al. 2010; Corbey et al. 2019; Emerson et al. 2021). However, there are likely Pu-containing phases other than PuO_2 in these sediments that impact Pu release but are present at concentrations below the detection limits of conventional solid phase characterization techniques. This is particularly the case in the Z9-4-11A sediments, where the nature of the Pu solubility-controlling phases may have been affected by harsher radiologic conditions, due to higher Pu concentrations, and greater mineral alteration, as indicated by an overlying sludge containing silicon and aluminum (Swanson 1973; Smith 1973; Delegard et al. 2019).

The dissolved Pu concentrations for Z9-4-5A sediments were more than an order of magnitude lower than PuO_2 solubility in the absence of sediments (Table 3b; Rai et al. 1980), although PuO_2 still controls solubility in some samples based on SI (including all major aqueous species measured in solution). Based on the predicted SIs, PuO_2(am,hyd), $PuPO_4$(am,hyd), and $Pu(HPO_4)_2$(am,hyd) phases control solubility for Z9-4-5A sediment, depending on the pH and available PO_4^{-3} (Tables 3 and 4) with a near 50/50 split between PuO_2 and Pu phosphate phases

(bolded values in Tables 3 and 4). As the pH is increased, and as PO_4^{3-} decreases, saturation is closer to PuO_2(am,hyd) (Table 4, Z9-4-5A-NA-AF) than Pu phosphate species. PuO_2(cr) is supersaturated (SI > 2.4) under all experimental conditions and is not expected to control solubility as it slowly converts to PuO_2(am,hyd) at the surface (Rai and Ryan 1982).

Aqueous Pu concentrations in equilibration with Z9-4-11A sediments are mostly below PuO_2 solubility in the absence of sediments (Figure 4b), although some samples were within the Pu colloid range estimated previously (Neck et al. 2007). Based on the SIs (Tables 3 and 4), Pu is in the range of saturation for PuO_2 in approximately half of the samples, while others most closely matched to Pu phosphate phases for solubility controls (bolded values). The smaller, less ordered PuO_2 particles in Z9-4-11A sediments likely result in an increase in the colloidal sized fraction (Emerson et al. 2021), which may also play a role in Pu release. In addition, PO_4^{3-} may be too low to convert the $PuO_{2(hyd)}$ to $PuPO_4$(am,hyd) in some samples. The maximum concentration in Z9-4-11A was 4.1×10^{-5} mol/L of PO_4^{3-}, compared to 6.6×10^{-3} mol/L in Z9-4-5A.

Previous microscopic and spectroscopic characterization of Z9-4-5A samples (Emerson et al., 2021) was consistent with large, ordered PuO_2 particles, but the SIs in Table 4 suggest that Pu phosphate phases are controlling solubility for most samples. Therefore, to further investigate the potential presence of Pu phosphate phases in Z9-4-5A sediments, samples were analyzed by STEM (Figure 5). The sediment contains PuO_2 particles ranging in size from nanometers to several micrometers (Figure 5a,b), with PCA of the STEM-EDS maps providing evidence for a secondary Pu-containing phase with a less well-defined structure. Further analysis with high resolution TEM identified phases consistent with Pu phosphate (see SM Figure S6). Figure S6d shows the ideal monoclinic, P 21/n structure for $PuPO_4$(am,hyd), with all the metal atoms forming planes in the (200) orientation, and the selected area electron diffraction pattern (Figure

S6c) supports the presence of nanoscale, crystalline Pu phosphate phases. These results confirm the earlier identification of an amorphous Fe-Pu-phosphate in some of these shallow sediments using electron microscopy (Buck et al., 2014). Thus, when sufficient phosphate is present, it is these $PuPO_4$(am,hyd) or $Pu(HPO_4)_2$(am,hyd) phases that control Pu solubility in Z9-4-5A sediments, not the larger, ordered PuO_2 particles. Because little phosphate is present naturally in the sediments and free inorganic phosphate was not in the Pu scrap or processing, it is likely that the source of the phosphate in the shallow sediments is from degradation of TBP and its first hydrolysis product, dibutyl phosphate (DBP), which was co-disposed to the Z-9 Trench in solvent cleanup (Delegard et al. 2019). It is hypothesized that, in the early life of the Z-9 Trench, PuO_2(am,hyd) may have controlled Pu solubility but, as more phosphate became available through degradation of TBP and DBP in later years, PuO_2(am,hyd) was replaced by more stable (less soluble) $PuPO_4$(am,hyd), which now controls the release of Pu to solution in some Z9-4-5A and Z9-4-11A samples.

SI values predict that the solutions contacted with the deeper Z-9 Trench sediments (B1HK) are saturated with respect to PuO_2(am,hyd) (Figure 4c), although concentrations were more than one order of magnitude lower than PuO_2(am,hyd) solubility in the absence of sediments (Figure 4a). As pH increases, Pu, Am, and PO_4^{3-} decrease such that Pu phosphate phases are undersaturated for both B1HK27 and B1HK42. For B1HK27, PuO_2(am,hyd) appears to be oversaturated (SI > 0), although they are still close to saturation. For the deepest sample (B1HK42), PuO_2(am,hyd) is controlling the Pu solubility (SI ~0.5). Though solid phase Pu concentrations are too low in these sediments for spectroscopic characterization, these results (Table 4) confirm that the sediments received ample Pu to reach saturation w.r.t. PuO_2 allowing it to control release of Pu (4×10^{-6} and 2×10^{-7} mol/L total Pu for B1HK-27 and B1HK-42, respectively, Emerson et al. 2021). This

is a similar conclusion to previous research on Pu-contaminated Savannah River Site sediments (Kaplan et al. 2006).

The overlay of pH and Eh measurements onto a Pourbaix diagram for Pu species in Figure 3 further highlights the complex processes controlling Pu release as Z9-4-5A measurements are near Pu-phosphate species, Z9-4-11A measurements are split between Pu-phosphate and PuO_2, and B1HK samples are near PuO_2 phases. The uncertainties in the values for Pu solubility in the shallow sediments (Z-9, Figure 4b) as compared to PuO_2 solubility suggest that the solubility controls are more complex than the initial PuO_2 phases disposed of to the subsurface. Therefore, the importance of phosphate in reducing the mobility of Pu must be considered, as it may have implications for long-term mobility, and could also be used for future remediation, with phosphate solutions or hydroxyapatite introduced as an amendment to limit Pu transport in the subsurface (SM Figures S9-10).

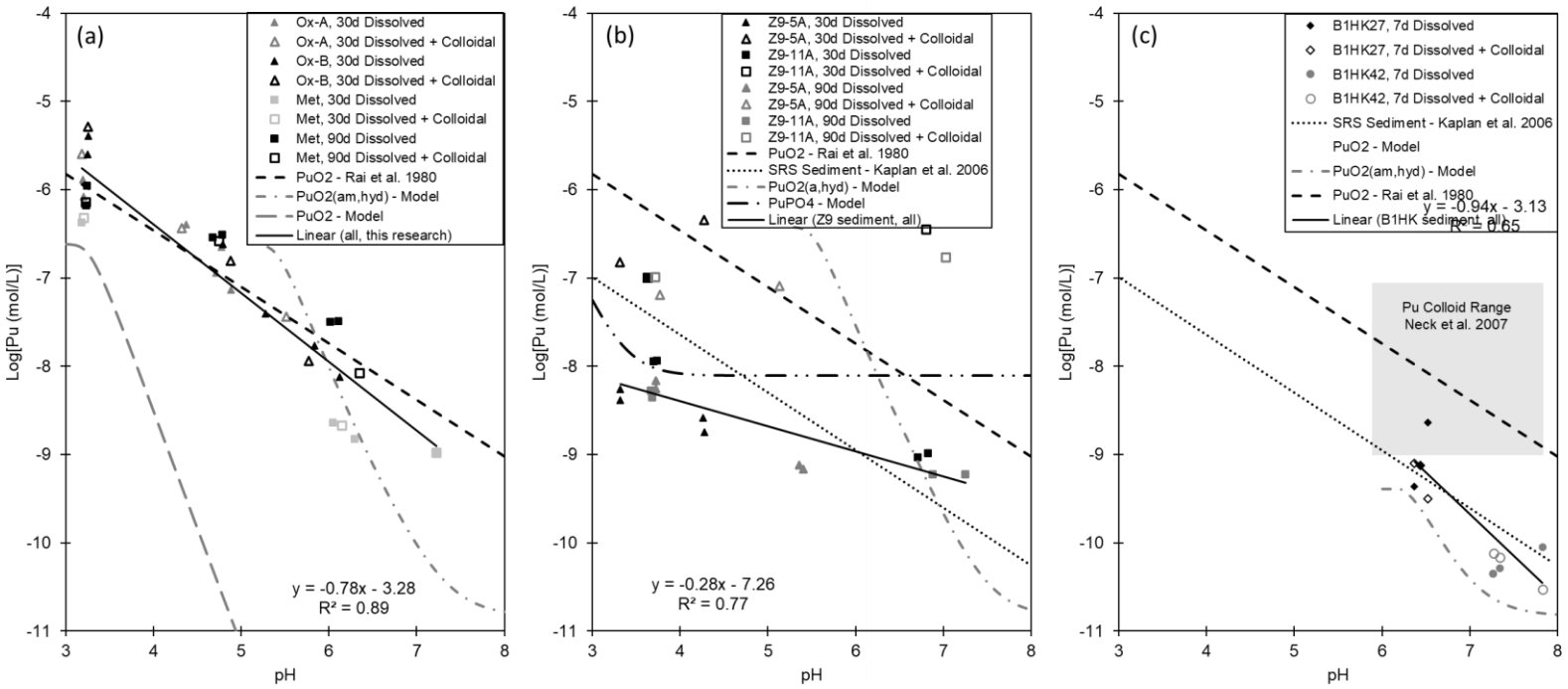

Figure 4: 30-day batch solubility experiments with (a) PuO_2 (*triangles* for Ox-A/B, *squares* for Met), (b) shallow contaminated Z9 sediments (*triangles* for Z9 30-day and *squares* for Z9 90-day),and (c) deeper contaminated B1HK sediments (*diamonds* for B1HK-27 and *circles* for B1HK42) with *filled* symbols representing dissolved species with acidification after filtration (AF) and *open* symbols representing dissolved and colloidal species with acidification before filtration (BF). Total aqueous Pu is compared to previous solubility measurements for PuO_2 in 0.0015 M $CaCl_2$ (Rai et al. 1980; *black dashed* line), Pu colloids (Neck et al. 2007; *light gray* box from pH 6-8), major species predicted in GWB model [PuO_2(am,hyd) as *dashed-dot gray line*, PuO_2(cr) as *dashed gray line*, and $PuPO_4$(am,hyd) as *dashed-dot black line*] based on the following samples for (a) Ox-B-3-BF with 6×10^{-6} M Pu in 10 mM $NaNO_3$, (b) Z-9-4-11A-6BF with 2.3×10^{-7} M Pu with major components measured in

solution, and (c) B1HK-27-BF with 4.3×10^{-10} M Pu with major components measured in solution], and a linear fit of Pu dissolution from Savannah River Site (SRS) sediments (Kaplan et al. 2006; *black dotted line*).

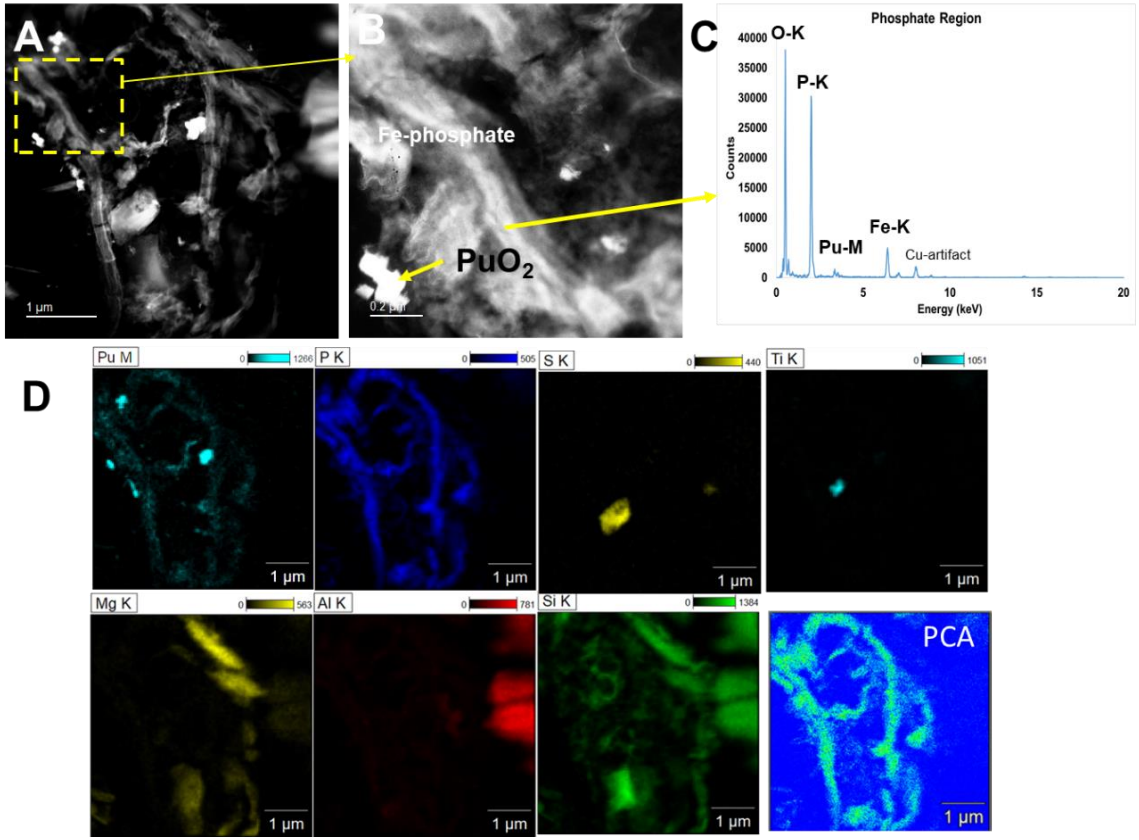

Figure 5: (A) STEM-HAADF Images of the plutonium bearing regions in thin-sectioned Z9-4-5A sediment showing two types of plutonium phases. (C) EDS analysis from the phosphate component containing detectable Pu. (D) Elemental maps, labeled; Pu-M, P-K, S-K, Ti-K, Mg-K, Al-K, Si-K, and PCA containing a secondary Pu phase.

Table 3: SIs for Am and Pu phases in Z-9 sediment equilibrated with DIW for 8 days without pH adjustment, with Pu, Am, PO_4^{3-} concentrations, pH, and Eh (in mV vs. SHE), **bolded** values indicate likely solubility controlling phases with average and standard deviation based on triplicates for B1HK samples and duplicates for Z9 samples, AF – acidified after filtration, BF – acidified before filtration.

Sample ID	SI PuO_2(cr)	SI PuO_2 (am,hyd)	SI $PuPO_4$ (am,hyd)	SI $Pu(HPO_4)_2$ (am,hyd)	SI $AmPO_4$ (am,hyd)	Pu (mole/L)	Am (mole/L)	PO_4^{3-} (mole/L)	pH	Eh (mV)
Z9-4-5A-AF	4.05 ± 2.52	-1.64 ± 2.52	1.89 ± 0.13	**0.53 ± 2.42**	**0.75 ± 0.10**	[1.1 ± 0.1] × 10^{-08}	[7.1 ± 1.0] × 10^{-09}	[1.20 ± 0.01] × 10^{-03}	3.31 ± 0.05	488 ± 0
Z9-4-5A-BF	5.84 ± 0.02	**0.15 ± 0.02**	1.87 ± 0.12	1.26 ± 0.12	**0.75 ± 0.12**	[5.5 ± 2.5] × 10^{-07}	[1.6 ± 0.5] × 10^{-08}			
Z9-4-11A-AF	7.76 ± 0.24	1.58 ± 0.46	**0.68 ± 0.02**	-1.95 ± 0.03	1.51 ± 0.03	[9.3 ± 2.9] × 10^{-08}	[4.2 ± 0.5] × 10^{-09}	[7.5 ± 0.9] × 10^{-05}	4.54 ± 0.10	448 ± 4
Z9-4-11A-BF	9.56 ± 1.03	3.88 ± 1.03	2.40 ± 0.70	**-0.32 ± 0.67**	2.40 ± 0.90	[1.4 ± 1.7] × 10^{-05}	[8.0 ± 9.5] × 10^{-08}			
B1HK27-AF	7.25 ± 0.40	**1.56 ± 0.40**	-4.86 ± 0.41	-8.81 ± 0.42	4.00 ± 0.21	[1.2 ± 1.0] × 10^{-09}	[1.4 ± 0.5] × 10^{-13}	[8.3 ± 0.2] × 10^{-06}	6.44 ± 0.08	444 ± 8
B1HK-27-BF	7.05 ± 0.20	**1.36 ± 0.20**	-5.05 ± 0.18	-9.00 ± 0.25	4.01 ± 0.19	[6.2 ± 2.7] × 10^{-10}	[1.3 ± 1.2] × 10^{-11}			
B1HK42-AF	4.86 ± 2.51	-0.86 ± 2.51				[6.1 ± 2.5] × 10^{-11}	[5.8 ± 4.1] × 10^{-14}	<EQL	7.48 ± 0.31	434 ± 5
B1HK42-BF	6.21 ± 0.21	**0.52 ± 0.21**				[5.8 ± 2.5] × 10^{-11}	[1.1 ± 0.0] × 10^{-11}			

<EQL – less than the estimated quantitation limit for PO_4^{3-} (2.4 × 10^{-06})

Table 4: SIs for Am and Pu phases in contaminated Z-9 sediments equilibrated with DIW for 30 days with adjustment to pH 3 and without adjustment (NA) with Pu, Am, PO_4^{3-} concentrations, pH, and Eh (in mV vs. SHE), **bolded** values indicate likely solubility controlling phases, BF – acidified prior to filtration to dissolve colloids, AF – acidified after filtration, average and standard deviation for two duplicate samples.

Sample	SI PuO_2(cr)	SI PuO_2 (am,hyd)	SI $PuPO_4$ (am,hyd)	SI $Pu(HPO_4)_2$ (am,hyd)	SI $AmPO_4$ (am,hyd)	Pu (mole/L)	Am (mole/L)	PO_4^{3-} (mole/L)	pH	Eh (mv)
Z9-4-5A-3-AF	6.46 ± 2.15	-0.73 ± 0.03	-0.76 ± 0.07	**-0.35 ± 0.01**	**1.31 ± 0.37**	[5.4 ± 0.7] × 10^{-09}	[1.5 ± 1.2] × 10^{-07}	[6.3 ± 0.2] × 10^{-04}	3.32 ± 0.00	569 ± 3
Z9-4-5A-3-BF	6.39	**0.71**	**0.65**	**1.08**	1.71	1.51 × 10^{-07}	3.34 × 10^{-07}	6.01 × 10^{-04}	3.31	571
Z9-4-5A-NA-AF	5.98 ± 0.05	**0.29 ± 0.05**	-0.62 ± 0.14	-1.19 ± 0.14	**1.53 ± 0.06**	[2.8 ± 0.3] × 10^{-09}	[2.5 ± 0.2] × 10^{-09}	[6.0 ± 0.1] × 10^{-04}	4.27 ± 0.01	510 ± 4
Z9-4-5A-NA-BF	8.14	2.45	1.58	**1.04**	1.98	4.52 × 10^{-07}	6.13 × 10^{-09}	6.61 × 10^{-04}	4.28	509
Z9-4-11A-3-AF	6.02 ± 0.06	**0.33 ± 0.06**	-2.96 ± 0.49	-4.29 ± 1.00	**-0.64 ± 0.45**	[1.3 ± 0.1] × 10^{-08}	[2.1 ± 0.1] × 10^{-08}	[1.0 ± 0.9] × 10^{-05}	3.72 ± 0.02	590.9 ± 0.3
Z9-4-11A-3-BF	6.82	**1.14**	-1.95	-2.54	**-0.56**	9.96 × 10^{-08}	1.54 × 10^{-08}	1.63 × 10^{-05}	3.63	601
Z9-4-11A-NA-AF	7.45 ± 0.05	1.74 ± 0.07	-5.61 ± 0.02	-7.49 ± 0.02	3.42 ± 0.19	[1.1 ± 0.1] × 10^{-9}	[2.8 ± 1.3] × 10^{-10}	[3.2 ± 0.9] × 10^{-05}	6.76 ± 0.08	514 ± 4
Z9-4-11A-NA-BF	9.95	4.26	-3.12	-4.84	4.63	3.55 × 10^{-07}	3.06 × 10^{-09}	4.10 × 10^{-05}	6.81	517

4.3.2 Am solubility controlling phases in contaminated sediments

Rai et al. (1981) previously measured ^{241}Am removal from the same sediment samples from near the Z-9 Trench bottom (Z9-4-5A and Z9-4-11A). However, ^{241}Am concentrations are increasing over time due to the decay of ^{241}Pu (half-life of 14.4 years). Figure 6c compares Z9-4-5A and Z9-4-11A batch experiments conducted previously by Rai et al. (1981; *black* line) with the ^{241}Am concentrations measured in near-surface Z-9 Trench sediments (Z9-4-5A and Z9-4-11A) and the deeper sediments (B1HK-27 and B1HK-42). In the acidic pH range, Am concentrations are similar to those found by Rai et al. (1981) for Z9 sediments; however, above pH 6, the dissolved Am fraction in Z9-4-11A sediments is significantly higher, and in B1HK sediments is significantly lower. The lower aqueous Am in the deeper B1HK sediments suggests different controls besides solubility.

The SI values calculated for Z9-4-5A for Am suggest that $AmPO_4$(am, hyd) likely controls release from these samples, just as $PuPO_4$(am,hyd) likely controls Pu concentrations (Table 3 and 4 and Figure 6a). The large stability region for $AmPO_4$(am, hyd) predicted in sediments in the presence of phosphate confirms the results for Z9-4-5A (Figure 6a). However, $AmPO_4$(am, hyd) is undersaturated in Z9-4-11A samples below pH 4 and significantly oversaturated above pH 4, indicating that $AmPO_4$(am, hyd) does not control Am solubility in Z9-4-11A sediments. Other unidentified phases may play a role in the release of Am from Z9-4-11A sediments (e.g., complexation with organic degradation products or precipitation in silica alteration products) due to the complexity of wastes disposed to the trench. We suggest that $AmPO_4$(am,hyd) may be the solubility controlling phase that was present in previous experiments by Rai et al. (1981), although thermodynamic constants were not yet available for this species.

Because PO_4^{3-} was below detection limits for B1HK-42 sediments (< 0.23 mg/L), $AmPO_4$(am, hyd) is unlikely to control Am concentrations and oversaturated SI values of ~ 4.0 were calculated. In the absence of phosphate (Figure 6b), no solubility-controlling phases are predicted for Am, with Am concentrations likely controlled by adsorption (Figure 6). Alternatively, there is the potential for $Pu_{(1-x)}Am_xO_2$ dissolution to control release of Am in the deeper sediments (Emerson et al. 2021; Neilson et al. 2021), as results suggest Pu release is controlled by PuO_2(am,hyd).

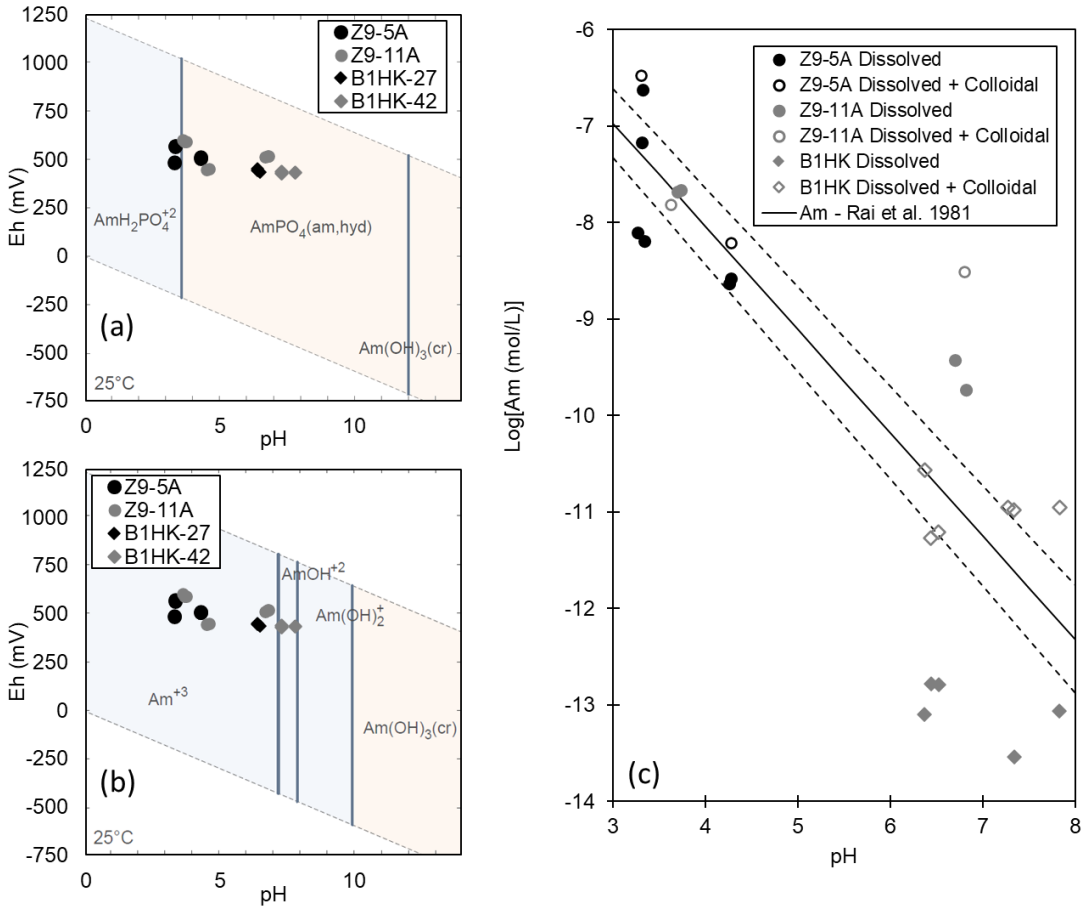

Figure 6: Am stability field diagrams based on characterization of aqueous supernatants from 30-day batch solubility experiments with Am-contaminated sediments from Z-9 Trench (sample Z9-4-11A-6BF with 3.70×10^{-10} M Am and 4.07×10^{-5} M PO_4), where *blue* regions represent dominant aqueous species and *yellow* regions represent dominant solid phase species as labeled with (a) inclusion of phosphate and (b) exclusion of phosphate with an overlay of pH and Eh results. In (c), batch solubility experiments with contaminated sediments (*black circles* for Z9-4-5A, *gray circles* for Z9-4-11A, and *black diamonds* for B1HK-27 and B1HK-42) with *filled* symbols representing dissolved species with acidification after filtration (AF) and *open* symbols representing dissolved and colloidal species with acidification before filtration (BF) for ^{241}Am with comparison to previous measurements for ^{241}Am in contaminated sediments from the Z9 Trench bottom (Rai et al. 1981; *black* line with 95% confidence intervals as *black dashed* lines). Note: Major constituents included from a specific sample, although predicted Pourbaix

diagrams were similar for all Am-contaminated sediments. Carbonate was excluded from this system. In equilibrium with air, carbonate species are not dominant until pH > 10 and, therefore, are not relevant to this research (see SM Figure S7b).

4.3.3 Impact of colloid formation on Pu and Am mobility in contaminated sediments

Significant colloidal Pu was not observed in PuO_2 solubility experiments in the absence of sediments (Figure 4a), showing that intrinsic PuO_2 colloids were not stable. However, nearly all sediment samples that were acidified prior to filtration had higher concentrations of Pu and Am (*open* symbols showing dissolved plus colloidal Pu and Am in Figures 4 and 6, respectively) than those which were filtered (*filled* symbols showing dissolved Pu and Am in Figures 4 and 6, respectively). This was likely the result of partial dissolution of pseudo colloids (e.g., aqueous Pu species or PuO_2 sorbed to natural colloids such as clays). While a few samples at pH > 6 fall within the range of PuO_2 intrinsic colloids (Figure 4), Neck et al. (2007) suggested that PuO_2 colloids were unlikely to play a role under acidic conditions. Positively charged intrinsic PuO_2 colloids and/or adsorbed Pu (as well as Am) would also likely adsorb to negatively charged natural colloids, e.g., smectite clay colloids, in the presence of sediments (Abdel-Fattah et al. 2013).

Though previous research has shown that natural colloids above pH 7 exhibit an intermediate stability in Hanford groundwater (Czigany et al. 2005), they are unlikely to sustain stability to the extent required for transport through the deep vadose zone to groundwater. Notably, the B1HK samples from deeper sediments below the Z-9 Trench did not contain a significant fraction of Pu in the colloidal size range (Figure 4c), supporting the hypothesis that Pu was not transported to these depths as intrinsic or pseudo-colloids.

5.0 CONCLUSIONS

The solubility of various forms of PuO_2 was investigated and compared with release of Pu from sediments contaminated by disposal of acidic, high salt wastes. PuO_2 solubility in the absence of sediments was consistent with that determined for hydrous, aged PuO_2 in previous work (Rai et al. 1980), including for different PuO_2 synthesis methods. However, at near-neutral pH, it took longer to reach equilibrium for larger (>100 μm) PuO_2 particle aggregates produced from Pu metal, suggesting surface area may control release rates.

Release of Pu from Z-9 Trench sediments at the Hanford Site is controlled by PuO_2(am,hyd) or Pu-phosphate [$PuPO_4$(am,hyd) or $Pu(HPO_4)_2$(am,hyd)] phases, depending on the pH and available phosphate. Pu solubility in shallow sediments was controlled by PuO_2(am,hyd), if the concentration of phosphate was low. When sufficient phosphate was present in shallow sediments, phases consistent with Pu phosphate were identified by high resolution TEM, confirming the potential for phosphate to control the long-term release of Pu from these sediments. Speciation modeling also confirmed the importance of these phases depending on the phosphate concentration, pH, and oxidation state of Pu (Figure 7a,b). The phosphate source was likely degradation of TBP, which was co-disposed to the Z-9 Trench. Release of Am from these shallow sediments is also controlled primarily by $AmPO_4$(am, hyd), provided sufficient phosphate, Am, and acidity is present (Figure 7c). The shift of shallow sediments from oxide to phosphate controls is likely due to changes in Pu and Am speciation over time depending on pH and available phosphate. The stability fields of solid phosphate-bearing Pu and Am phases, respectively, extend into the acidic pH range, depending on available phosphate.

Pu and Am were initially mobile and transported to deeper sediments beneath the Z-9 Trench in the acidic wastes. As wastes were neutralized within the soil profile, Pu was precipitated as PuO_2. Pu release from these deeper sediments, which contain orders of magnitude less phosphate

than the shallow sediment, is thus controlled by PuO_2(am,hyd) solubility. Am release behavior in deeper sediments is more complex, and potentially controlled by desorption from sediment minerals, dissolution from PuO_2 particles following ^{241}Am daughter in-growth, or other unidentified solubility-controlling phases. Above pH 6 in deeper sediments, Am solubilities diverge from those for $AmPO_4$(am, hyd), suggesting that temporal changes in Am speciation can be influenced by: (i) in-growth of daughter products; (ii) interactions with breakdown products of organics from the waste; and/or (iii) formation of complexes with carbonate in the subsurface.

No evidence was found for intrinsic Pu or Am colloids in the absence of sediment, but Pu and Am were associated with the colloidal size fraction, likely as pseudo colloids, in shallow sediments. However, deeper sediments from beneath the Z-9 Trench did not contain a significant fraction of Pu in the colloidal size range, supporting previous research showing that colloids (intrinsic or pseudocolloids) are unlikely to reach groundwater once acid from the waste is neutralized with depth and sediments are at neutral pH (Czigany et al. 2005). Thus, colloids are unlikely to represent a significant Pu transport vector to groundwater in Hanford site sediments, but the potential impact of Pu transport in association with pseudocolloids may need to be considered at other sites.

The solubility controls identified in this study can be used to explain Pu and Am historical transport behavior and to assess the potential for future subsurface transport and remediation. These newly identified solubility controls are likely applicable to other locations within the Hanford Site, including the Z-1A tile field and the Z-18 crib (Owens 1981), as well as other sites with releases of acidic waste with Pu and Am (e.g., Los Alamos, NM and Savannah River Site, SC) (Batuk et al. 2015; Carlton et al. 1992).

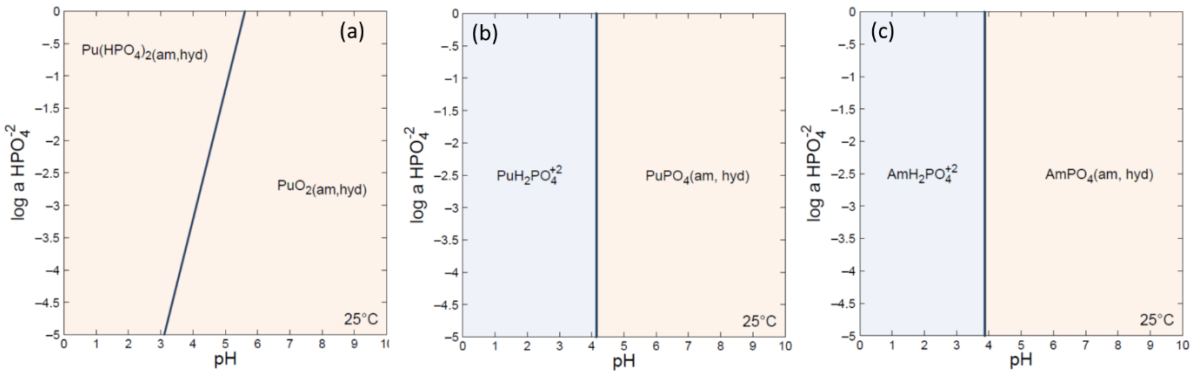

Figure 7: Predominance diagrams for (a) 1×10^{-11} mol/L as Pu(IV), (b) 1×10^{-11} mol/L as Pu(III), and (c) 1×10^{-10} mol/L Am with variable concentrations of phosphate (as logarithm of concentration in mol/L) based on constituents analyzed in 30-day batch equilibration of Z9-4-11A sediments (sample Z9-4-11A-NA-BF), Note: Oxidation states were fixed in these models to highlight the importance of both +3 and +4 solid phases for Pu. Similar diagrams were predicted for other sediment samples and carbonate may play a role at high pH (SM Figure S6).

6.0 ACKNOWLEDGEMENTS

This document was prepared under the Deep Vadose Zone – Applied Field Research Initiative at Pacific Northwest National Laboratory. The Pacific Northwest National Laboratory is operated by Battelle Memorial Institute for the DOE under Contract DE-AC05-76RL01830. The authors acknowledge James Szecsody and Amanda Lawter for their careful review and Matthew Wilburn for technical editing. Lawrence Livermore National Laboratory authors' contributions were supported by the Department of Energy, Office of Science, Biological and Environmental Research, Subsurface Biogeochemical Research program (SCW1053) and performed under the auspices of the U.S. Department of Energy by Lawrence Livermore National Laboratory under Contract DE-AC52-07NA27344.

7.0 REFERENCES

Abdel-Fattah, AI, D Zhou, H Boukhalfa, S Tarimala, SD Ware, and AA Keller. 2013. "Dispersion stability and electrokinetic properties of intrinsic plutonium colloids: Implications for subsurface transport." *Environmental Science and Technology* 47:5626-5634. https://doi.org/10.1021/es304729d

Altmaier, M, X Gaona, and T Fanghänel. 2013. "Recent advances in aqueous actinide chemistry and thermodynamics." *Chemical Reviews* 113:901-943. https://doi.org/10.1021/cr300379w

Ames LL. 1974. *Characterization of Actinide Bearing Soils: Top Sixty Centimeters of 216-Z-9 Enclosed Trench*. BNWL-1812, Battelle Pacific Northwest Laboratories, Richland, WA. https://www.osti.gov/biblio/4313915-characterization-actinide-bearing-soils-top-sixty-centimeters-enclosed-trench

Barr, MJ, MW Urie, JL Daniel, and SJ Mayhan. 1970. Characterization of Some UO_2 and PuO_2 Powders. BNWL-1441, Battelle Memorial Institute, Richland, WA. http://www.osti.gov/scitech//servlets/purl/4102315/

Batuk ON, SD Conradson, ON Aleksandrova, H Boukhalfa, BE Burakov, DL Clark, KR Czerwinski, AR Felmy, JS Lezama-Pacheco, SN Kalmykov, DA Moore, BF Myasoedov, DT Reed, DD Reilly, RC Roback, IE Vlasova, SM Webb, and MP Wilkerson. 2015. "Multiscale speciation of U and Pu at Chernobyl, Hanford, Los Alamos, McGuire AFB, Mayak, and Rocky Flats." *Environmental Science and Technology* 49:6474-6486. https://doi.org/10.1021/es506145b

Bethke C and S Yeakel. 2010. The Geochemist's Workbench, Release 8.0, Reference Manual. Urbana, Illinois.: Hydrogeology Program.

BHI – Bechtel Hanford, Inc. 1995. DNAPL Investigation Report. BHI-00431, Rev. 0, Richland, Washington. https://pdw.hanford.gov/download/e5514123-c614-44ac-8b3e-fa5110e89bc4

Bonato L, M Viro, T Dumas, A Mesbah, E Dalodiere, OD Blanco, T Wiss, X Le Goff, M Odorico, D Prieur, A Rossberg, L Venault, N Dacheux, P Moisy, and SI Nikitenko. 2020. "Probing the local structure of nanoscale actinide oxides: a comparison between PuO_2 and ThO_2 nanoparticles rules out PuO_{2+x} hypothesis. *Nanoscale Adv.* 2, 214-224. https://doi.org/10.1039/C9NA00662A

Brodeur JR, RK Price, RD Wilson, and CJ Koizumi. 1993. *Results of Spectral Gamma-Ray Logging of Select Boreholes for the Aggregate Area Management Study*. WHC-SD-EN-TI-021, Rev. 0, Westinghouse Hanford Company, Richland, WA https://pdw.hanford.gov/document/D196111465

Buck EC, DA Moore, KR Czerwinski, SD Conradson, ON Batuk, and AR Felmy. 2014. "Nature of nano-sized plutonium particles in soils at the Hanford Site." *Radiochimica Acta* 102(12):1059-1068. https://doi.org/10.1515/ract-2013-2103

Cantrell KJ, RJ Serne, and GV Last. 2003. Hanford Contaminant Distribution Coefficient Database and Users Guide. PNNL-13895, Rev. 1, Pacific Northwest National Laboratory,

Richland, Washington.
https://www.pnnl.gov/main/publications/external/technical_reports/PNNL-13895rev1.pdf

Cantrell KJ and RG Riley. 2008. A Review of Subsurface Behavior of Plutonium and Americium at the 200-PW-1/3/6 Operable Units. PNNL-SA-58953, Pacific Northwest National Laboratory, Richland, Washington.
https://www.pnnl.gov/main/publications/external/technical_reports/PNNL-SA-58953.pdf

Cantrell KJ, KN Geiszler, and BW Arey. 2008. Plutonium Mobility Studies: 216-Z-9 Trench Sample Analysis Results. PNNL-17839, Pacific Northwest National Laboratory, Richland, WA.
https://www.pnnl.gov/main/publications/external/technical_reports/PNNL-17839.pdf

Cantrell KJ. 2009. Transuranic Contamination in Sediment and Groundwater at the U.S. DOE Hanford Site. PNNL-18640, Pacific Northwest National Laboratory, Richland, Washington.
https://www.pnnl.gov/main/publications/external/technical_reports/PNNL-18640.pdf

Cantrell KJ and AR Felmy. 2012. Plutonium and Americium Geochemistry at Hanford: A Site-Wide Review. PNNL-21651, Pacific Northwest National Laboratory, Richland, WA.
https://www.pnnl.gov/main/publications/external/technical_reports/pnnl-21651.pdf

Carlton WH, AG Evans, CE Murphy, JE Pinder, and RN Strom. 1992. *Assessment of Plutonium in the Savannah River Site Environment*. WSRC-RP-92-879-Rev.1, Savannah River National Laboratory, Aiken, SC. https://doi.org/10.2172/10196102

Conradson SD, BD Begg, DL Clark, C Den Auwer, FJ Espinosa-Faller, PL Gordon et al. 2003. "Speciation and unusual reactivity in the PuO_{2+x}." *Inorg. Chem.* 42(12), 3715-3717. https://doi.org/10.1021/ic026044l

Conradson SD, BD Begg, DL Clark, C Den Auwer, M Ding, PK Dorhout et al. 2004. "Local and nanoscale structure and speciation in the $PuO_{2+x-y}(OH)_{2y}{\cdot}zH_2O$ system." *J. Am. Chem. Soc*. 126(41), 13,443-13,458. https://doi.org/10.1021/ja049192e

Conradson SD, BD Begg, DL Clark, C Den Auwer, M Ding, PK Dorhout et al. 2005. "Charge distribution and local structure and speciation in the UO_{2+x} and PuO_{2+x} binary oxides for x ≤0.25." *J. Solid State Chem.* 178(41), 521-535. https://doi.org/10.1016/j.jssc.2004.09.029

Corbey, JF, DD Reilly, LE Sweet, and TG Lach. 2019. "Extraction of plutonium-containing microcrystals from Hanford soil using a focused ion beam for single-crystal X-ray diffraction analysis." *Journal of Applied Crystallography*. 52:1422-1252. https://doi.org/10.1107/S1600576719012299

Corbin RA, BC Simpson, MJ Anderson, WF Danielson III, JG Field, TE Jones, and CT Kincaid. 2005. *Hanford Soil Inventory Model, Rev. 1*. RPP-26744, CH2M HILL Hanford Group, Richland, Washington. https://pdw.hanford.gov/document/0081114H

Czigany, S, M Flury, and JB Harsh. 2005. “Colloid stability in vadose zone Hanford sediments.” *Environmental Science and Technology* 39:1506-1512. https://doi.org/10.1021/es048714n

Deblonde, G.J.P., Kersting, A.B. and Zavarin, M. (2020) “Open questions on the environmental chemistry of radionuclides.” *Communications Chemistry* 3(167). https://doi.org/10.1038/s42004-020-00418-6

Delegard CH, HP Emerson, KJ Cantrell, and CI Pearce. 2019. *Generation and Characteristics of Plutonium and Americium Contaminated Soils and Underlying Waste Sites at Hanford*. PNNL-29203, Pacific Northwest National Laboratory, Richland, WA.

DOE/RL. 2007. *Remedial Investigation Report for the Plutonium/Organic-Rich Process Condensate/ Process Waste Group Operable Unit: Includes the 200-PW-1, 200-PW-3, and 200-PW-6 Operable Units*. DOE/RL-2006-51, Rev. 0, U.S. Department of Energy, Richland Operations Office, Richland, Washington. https://pdw.hanford.gov/arpir/index.cfm/viewDoc?accession=DA05807591

DOE/RL. 2015. *Remedial Design/Remedial Action Work Plan for the 200-CW-5, 200-PW-1, 200-PW-3, and 200-PW-6 Operable Units*. DOE/RL-2015-23, Rev. 0, U.S. Department of Energy, Richland Operations Office, Richland, Washington. https://pdw.hanford.gov/document/0076381H

Emerson, HP, CI Pearce, CH Delegard, KJ Cantrell, MMV Snyder, M-L Thomas, BN Gartman, MD Miller, CT Resch, SM Heald, AE Plymale, DD Reilly, SA Saslow, W Nelson, S Murphy, M

Zavarin, AB Kersting, VL Freedman. 2021. “Influences on subsurface plutonium and americium migration.” *ACS Earth and Space Chemistry*. 5(2), 279-294. https://doi.org/10.1021/acsearthspacechem.0c00277

Farr DJ, RK Schulze, and MP Neu. 2004. “Surface chemistry of Pu oxides.” *J. Nucl. Mater*. 328(2-3), 124-136. https://doi.org/10.1016/j.jnucmat.2004.04.001

Fecht KR, GV Last, and KR Price. 1977. *Evaluation of Scintillation Probe Profiles from 200 Area Crib Monitoring Wells*. ARH-ST-156, Volumes I, II, and III, Atlantic Richfield Hanford Company, Richland, Washington.d https://www.osti.gov/servlets/purl/7085590; https://www.osti.gov/servlets/purl/7085589/; https://www.osti.gov/servlets/purl/7284214

Felmy AR, KJ Cantrell, and SD Conradson. 2010. “Plutonium Contamination Issues in Hanford Soils and Sediments: Discharges from the Z-Plant (PFP) Complex.” *Physics and Chemistry of the Earth* 35:292-297. http://dx.doi.org/10.1016/j.pce.2010.03.034

Finnegan, DL, SM Bowen, JL Thompson, CM Miller, PL Baca, LF Olivas, CG Geoffrion, DK Smith, W Goishi, BK Esser, JW Meadows, N Namboodiri, and JF Wild. 2016, *Nevada National Security Site Underground Radionuclide Inventory, 1951-1992: Accounting for Radionuclide Decay through September 30, 2012*. LA-UR-16-21749, Los Alamos National Laboratory, Los Alamos, New Mexico. https://permalink.lanl.gov/object/tr?what=info:lanl-repo/lareport/LA-UR-16-21749

Gephart RE. 2010. “A Short History of Waste Management at the Hanford Site.” *Physics and Chemistry of the Earth* 35:298–306. https://doi.org/10.1016/j.pce.2010.03.032

Gerber MS. 1997. *History and Stabilization of the Plutonium Finishing Plant (PFP) Complex, Hanford Site*. HNF-EP-0924, Fluor Daniel Hanford, Incorporated, Richland, Washington. http://www.osti.gov/scitech/biblio/325360

Greintz, RM, and DH Neal. 1978. *Plutonium(IV) Oxalate Precipitation and Calcination Process for Plutonium Nitrate to Oxide Conversion*. RFP-2602, Rockwell International, Golden, CO. http://sti.srs.gov/fulltext/RFP-2602.pdf

Guillaumont R, FJ Mompean, T Fanghänel, J Fuger, I Grenthe, V Neck, DA Palmer, and ML Rand. 2003. Chemical Thermodynamics, Vol. 5. Update on the Chemical Thermodynamics of Uranium, Neptunium, Plutonium, Americium and Technetium, OECD, NEA-TDB, Elsevier, North Holland, Amsterdam. https://www.oecd-nea.org/dbtdb/pubs/vol5-update-combo.pdf

Grenthe, I, X Gaona, AV Plyasunov, WH Runde, RJM Konings, EE Moore, L Rao, B Grambow, and AL Smith. 2020. Chemical Thermodynamics, Vol. 14. Second update on the chemical thermodynamics of uranium, neptunium, plutonium, americium, and technetium, OECD, NEA-TDB, North Holland, Amsterdam. https://www.oecd-nea.org/jcms/pl_46643/second-update-on-the-chemical-thermodynamics-of-u-np-pu-am-and-tc?details=true

Haschke JM. 1992. *Evaluation of Source-Term Data for Plutonium Aerosolization*. LA-12315-MS, Los Alamos National Laboratory, Los Alamos, NM. http://lib-www.lanl.gov/cgibin/getfile?00193529.pdf

Judson BF, KM Harmon, LE Bruns, BA Chandler, FF Cole, HW Crocker, RB Guenther, WL Lyon, and RW McKee. 1956. *Semi-Works Operation of the RECUPLEX Facility – Volumes 1 and 2*. HW-44776 VOL1 and VOL2, Hanford Atomic Products Operation, Richland, Washington. https://reading-room.labworks.org/Files/GetDocument.aspx?id=D199117620 and https://reading-room.labworks.org/Files/GetDocument.aspx?id=D199117622

Judson BF. 1958. "Plutonium Recovery by a Reflux Solvent-Extraction System." Chapter 7-1 of *Progress in Nuclear Energy Series III – Process Chemistry*, Volume 2, FR Bruce, JM Fletcher and HH Hyman, editors, Pergamon Press, New York, New York. See also HW-49441 A, http://reading-room.labworks.org/Files/GetDocument.aspx?id=D8277166

Kanellakopulos, B, E Dornberger, J Müller, F Baumgärtner, U Benedict, and D Dufour. 1983. *Über die Löslichkeit von Plutoniumdioxid in Salpetersäure*. KFK-3353, Kernforschungszentrum Karlsruhe, Karlsruhe, Germany. http://bibliothek.fzk.de/zb/kfkberichte/KFK3353.pdf. In translation as Dissolution of Plutonium Dioxide in Nitric Acid, LA-UR-99-4169, Los Alamos National Laboratory, Los Alamos, NM.

Kaplan, DI, BA Powell, L Gumapas, JT Coates, RA Fjeld, and DP Diprete. 2006. “Influence of pH on plutonium desorption/solubilization from sediment.” *Environmental Science and Technology*, 40: 5937-5942. https://doi.org/10.1021/es060523s

Lemire RJ, J Fuger, H Nitsche, P Potter, MH Rand, J Rydbrg, K Spahiu, JC Sullivan, WJ Ullman, P Vitorge, and H Wanner. 2001. Chemical Thermodynamics, Vol. 4. Chemical Thermodynamics of Neptunium and Plutonium, OECD, NEA-TDB, Elsevier, North Holland, Amsterdam. https://www.oecd-nea.org/dbtdb/pubs/vol4-neptunium-plutonium.pdf

Lloyd MH and RG Haire. 1968. “A Sol-Gel Process for Preparing Dense Forms of PuO_2”. *Nuclear Applications* 5:114-122. https://doi.org/10.13182/NT68-A28040

Moseley JD and RO Wing. 1965. Properties of Plutonium Dioxide. RFP-503, The Dow Chemical Company, Golden, CO. http://www.osti.gov/scitech/biblio/4613823

Neck V and JI Kim. "Solubility and hydrolysis of tetravalent actinides." *Radiochimica Acta* 89.1 (2001): 1-16. https://doi.org/10.1524/ract.2001.89.1.001

Neck V, M Altmaier, A Seibert, JI Yun, CM Marquardt, T Fanghänel. 2007. Solubility and redox reactions of Pu(IV) hydrous oxide: Evidence for the formation of PuO_{2+x}(s,hyd). *Radiochim. Acta* 95, 193-207. https://doi.org/10.1524/ract.2007.95.4.193

Neck V, M Altmaier, T Fanghänel. 2007b. Solubility of plutonium hydroxides/hydrous oxides under reducing conditions and in the presence of oxygen. *C. R. Chimie* 10, 959-977. https://doi.org/10.1016/j.crci.2007.02.011

Neilson, WD, H Steele, and ST Murphy. 2021. Evolving Defect Chemistry of $(Pu,Am)O_{2\pm x}$. *JPCC*, *125* (28), 15560-15568. DOI: 10.1021/acs.jpcc.1c03274

Owens, KW. 1981. *Existing Data on the 216-Z Liquid Waste Sites*. RHO-LD-114. Rockwell Hanford Operations, Richland, WA. https://www.osti.gov/servlets/purl/5703558

Powell, BA, RA Fjeld, DI Kaplan, JT Coates, and SM Serkiz. 2004. $Pu(V)O_2^+$ adsorption and reduction by synthetic magnetite (Fe_3O_4). *Environmental Science and Technology* 38: 6016-6024. https://doi.org/10.1021/es049386u

Price, SM and LL Ames. 1975. *Characterization of Actinide-Bearing Sediments Underlying Liquid Waste Disposal Facilities at Hanford*. ARH-SA-232, Atlantic Richfield Hanford Company, Richland, Washington. https://inis.iaea.org/collection/NCLCollectionStore/_Public/07/238/7238004.pdf?r=1&r=1

Rai D, RJ Serne, and DA Moore. 1980. "Solubility of Plutonium Compounds and Their Behavior in Soils." *Soil Science Society of America Journal* 44(3):490-495. https://doi.org/10.2136/sssaj1980.03615995004400030010x

Rai, D, RG Strickert, and JL Ryan. 1980b. “Alpha Radiation Induced Production of HNO_3 during Dissolution of Pu Compounds”. *Inorganic and Nuclear Chemistry Letters* 16:551-555. https://doi.org/10.1016/0020-1650(80)80009-2

Rai D, RG Strickert, DA Moore, and RJ Serne. 1981. “Influence of an Americium Solid Phase on Americium Concentrations in Solutions.” *Geochimica et Cosmochimica Acta* 45:2257-2265. https://doi.org/10.1016/0016-7037(81)90075-2

Rai D and JL Ryan. 1982. “Crystallinity and solubility of Pu(IV) oxide and hydrous oxide in aged aqueous suspensions.” *Radiochimica Acta* 30(4):213-216. https://doi.org/10.1524/ract.1982.30.4.213

Rai, D, AR Felmy, and RW Fulton. 1992. “Solubility and ion activity product of $AmPO_4 \cdot xH_2O$(am).” *Radiochimica Acta*, 56, 7−14. https://doi.org/10.1524/ract.1992.56.1.7

Silva, RJ and H Nitsche. 1995. “Actinide Environmental Chemistry.” *Radiochimica Acta* 70/71: 377-396. https://doi.org/10.1524/ract.1995.7071.s1.377

Skipperud L, B Salbu, DH Oughton, E Drozcho, Y Mokrov, and P Strand. 2005. “Plutonium contamination in soils and sediments at Mayak PA, Russia.” *Health Physics* 89(3)255-265. https://doi.org/10.1097/01.HP.0000165449.06373.b0

Smith AE. 1973. *Nuclear Reactivity Evaluations of 216-Z-9 Enclosed Trench*. ARH-2915, Atlantic Richfield Hanford Company, Richland, Washington. https://inis.iaea.org/collection/NCLCollectionStore/_Public/05/120/5120615.pdf

Swanson JL. 1973. *Nature of Actinide Species Retained by Sediments at Hanford: Interim Progress Report*. BNWL-B-296, Battelle Pacific Northwest Laboratories, Richland, WA. https://www.osti.gov/biblio/4374249-nature-actinide-species-retained-sediments-hanford-interim-progress-report

Tasi A, X Gaona, D Fellhauer, M Bottle, J Rothe, K Dardenne, D Schild, M Grive, E Coas, J Bruno, K Kallstrom, M Altmaier and H Geckeis. 2018. "Redox behavior and solubility of plutonium under alkaline, reducing conditions." *Radiochimica Acta* 106(4):259-279. https://doi.org/10.1515/ract-2017-2870

Vauchy, R, A Joly, and C Valot. 2017. "Lattice thermal expansion of $Pu_{1-y}Am_yO_{2-x}$ plutonium-americium mixed oxides." *Journal of Applied Crystallography* 50:1782-1790. https://doi.org/10.1107/S1600576717014832

Zhao, P, M Zavarin, Z Dai, and AB Kersting. 2020. "Stability of plutonium oxide nanoparticles in the presence of montmorillonite and implications for colloid facilitated transport." *Applied Geochemistry*. 122: 104725-104735. https://doi.org/10.1016/j.apgeochem.2020.104725